Available online at www.sciencedirect.com
ScienceDirect
Journal of Sound and Vibration 318 (2008) 428–460
JOURNAL OF SOUND AND VIBRATION
www.elsevier.com/locate/jsvi

Analysis of axisymmetric shell structures under axisymmetric loading by the flexibility method

Troy Alvin Smith

US Army Research, Development, and Engineering Command, Aviation and Missile Research, Development, and Engineering Center, Redstone Arsenal, Alabama 35898, USA

Received 2 December 2005; received in revised form 22 January 2008; accepted 18 February 2008
Handling Editor: S. Bolton
Available online 15 August 2008

Abstract

A method is developed for the static stress and deformation analysis of axisymmetric shells under axisymmetric loading by reduction of the shell to ring sections. In particular, the wall thickness of the shell may vary and the method is applicable to the analysis of shells with irregular meridional geometry. Explicit expressions for the influence coefficients for each ring element are derived. In the development of these expressions, exact evaluation of stresses in the circumferential direction of the ring is used. The distribution of stresses in the meridional direction of the ring element is assumed to be linear with each element. By using the derived influence coefficients, the unknown forces at the junctures of the ring elements are found by the standard flexibility method of indeterminate structural analysis. Subsequently, the displacements and internal stresses are determined. Example solutions for a flat circular plate under transverse loading and for a cylindrical shell under a boundary edge loading show excellent agreement with solutions found by solving the governing differential equations.

1. Introduction

In the absence of closed-form static or dynamic solutions for the general shell, several investigators have obtained solutions for both the static problem and the dynamic problem by numerical methods. Included in these investigators were Penny [1], who solved the symmetric bending problem of a general shell in 1961 by finite differences; Radkowski et al. [2], who solved the axisymmetric static problem in 1962 by finite differences; and Budiansky and Radkowski [3], who used finite difference methods to solve the unsymmetrical static bending problem in 1963.

In 1964, Kalnins [4] also solved the static problem of rotationally symmetric shells of revolution subjected to both symmetrical and nonsymmetrical loading. Beginning with the equations of the linear classical bending theory of shells, in which the thermal effects were included, he derived a system of eight first-order ordinary differential equations that were solved by direct numerical integration over preselected segments of the shell. The resulting system of matrix equations obtained by providing continuity of the fundamental variables at the segmental division points was solved by Gaussian elimination.

The solution for the free vibration characteristics of rotationally symmetric shells with meridional variations in the shell parameters by means of his multisegment direct numerical integration approach was also obtained

0022-460X/$ - see front matter
doi:10.1016/j.jsv.2008.02.056

Nomenclature

a flexibility matrix for the base structure, Fig. 13

a_{ij} deflection of base structure in coordinate i due to a unit value of force in coordinate j, elements of flexibility matrix a

A cross-sectional area of ring element

c value of coordinate y' at coordinate 1, Fig. 1

d value of coordinate y' at coordinate 2, Fig. 1

D_{i0} deflection of base structure in coordinate i due to a combined external loading and temperature change, elements of column matrix of displacements with $F = 0$

E Young's modulus

F column matrix of redundant forces

F'_1 unit virtual longitudinal force per unit length applied at ring coordinate 1

h height of ring element measured parallel to ring element axis of symmetry

H_1 radial force per unit length applied at ring coordinate 1

H_2 radial force per unit length applied at ring coordinate 2

H'_1 unit virtual radial force per unit length applied at ring coordinate 1

H'_2 unit virtual radial force per unit length applied at ring coordinate 2

H_p radial load per unit length at R_3 due to external pressure

H_P^{T} total circumferential radial loading from H_P

$I_{z'}$ moment of inertia of ring cross section about z' axis

ℓ meridional length of ring element, Fig. 1

L longitudinal load per unit length applied at ring coordinate 1

$M_{z'}$, $M_{y'}$ induced internal moments about z' and y' axes, respectively, due to applied loadings

M_j total internally redundant meridional moment in coordinate j of the base structure

$m_{y'}$ virtual moment applied about y' axis at points A and B, Fig. 2

p uniform pressure on ring element surface

P_i total internally redundant radial force in coordinate i of the base structure

Q temperature rise of ring

R radius of centroid of ring element cross section

R_1 radius of ring element cross section at ring coordinate 1

R_2 radius of ring element cross section at ring coordinate 2

R_3 radius of center of pressure for uniform pressure on outer face of ring element

s variable distance measured along ring element meridian from coordinate 1

S direct force due to radially applied loads

t thickness of ring element of rectangular cross section

t_1 thickness of ring element measured normal to meridional centerline at coordinate 1

t_2 thickness of ring element measured normal to meridional centerline at coordinate 2

T torque per unit length about centroid of ring cross section

T_p torque per unit length about centroid of ring cross section due to external pressure

T_L torque per unit length about centroid of ring cross section due to L

T_{01} torque per unit length about centroid of ring cross section due to combined pressure and longitudinal loading with pressure loading resisted at R_1

T_{02} torque per unit length about centroid of ring cross section due to combined pressure and longitudinal loading with pressure loading resisted at R_2

T_3 meridional moment per unit length applied at ring coordinate 3

T_4 meridional moment per unit length applied at ring coordinate 4

T'_3 unit virtual meridional moment per unit length applied at ring coordinate 3

T'_4 unit virtual meridional moment per unit length applied at ring coordinate 4

V_{p1} longitudinal load per unit length resisted at ring coordinate 1 due to pressure loading

V_{p2} longitudinal load per unit length resisted at ring coordinate 2 due to pressure loading

V_p longitudinal load as force per unit length at R_3 due to external pressure

V_p^T total circumferential loading V_p

α angle between plane of middle surface of ring element and axis of symmetry of the element

β coefficient of thermal expansion of ring material

δ_{iH_1} deflection of ring element in ring coordinate i due to H_1

δ_{iH_2} deflection of ring element in ring coordinate i due to H_2

δ_{iT_3} deflection of ring element in ring coordinate i due to T_3

δ_{iT_4} deflection of ring element in ring coordinate i due to T_4

δ_{VH_1} change of length of ring element in longitudinal direction due to H_1

δ_{VH_2} change of length of ring element in longitudinal direction due to H_2

δ_{VT_3} change of length of ring element in longitudinal direction due to T_3

δ_{VT_4} change of length of ring element in longitudinal direction due to T_4

δ_{ij} deflection of ring element in ring coordinate i due to a unit value of force in coordinate j

δ_{Vj} change of length of ring element in longitudinal direction due to a unit of force in coordinate j

δ_{i0} deflection of ring element in ring coordinate i due to external loading only

δ_{V0} change of length of ring element in longitudinal direction due to external loading only

δ_{iT} deflection of ring element in ring coordinate i due to temperature change

δ_{VT} change of length of ring element in longitudinal direction due to temperature change

$\delta_{ij}^{(n)}$ deflection of ring element in ring coordinate i due to a unit value of force in coordinate j for ring associated with the number n

$\Delta_{i0}^{(n)}$ deflection of ring element in ring coordinate i due to combined external loading and temperature change for ring associated with the number n

Δ_{i0} deflection of ring element in ring coordinate i due to combined external loading and temperature change

Δ_{V0} change of length of ring element in longitudinal direction due to combined external loading and temperature change

$\Delta_j^{(n)}$ displacement of the nodal line coordinate j for the ring element n due to all effects

$\Delta_{y'}$ change in longitudinal length of structure due to all effects

$\in_x$ strain in circumferential direction of ring element

$\in_y$ strain in meridional direction of ring element

$\in_{x(j)}$ strain in circumferential direction of ring element due to j

$\in_{y(j)}$ strain in meridional direction of ring element due to j

$\in_{(j)}$ strain in ring element due to j

$\in_{(0)}$ strain in ring element due to external loading only

$\in_{x(AA)}^{(n)}$ strain in circumferential direction at point AA of the ring element n

$\in_{x(BB)}^{(n)}$ strain in circumferential direction at point BB of the ring element n

v Poisson's ratio

σ_x stress in circumferential direction of ring element

σ_y stress in meridional direction of ring element

$\sigma_{x(j)}$ stress in circumferential direction of ring element due to j

$\sigma_{y(j)}$ stress in meridional direction of ring element due to j

$\sigma_{(j)}$ stress in ring element due to j

$\sigma_{y(AA)}^{(n)}$ meridional stress at point AA of the ring element n

$\sigma_{y(BB)}^{(n)}$ meridional stress at point BB of the ring element n

$\sigma_x(M_{z'})$ stress σ_x due to $M_{z'}$, Eq. (2)

$\sigma_x(M_{y'})$ stress σ_x due to $M_{y'}$, Eq. (3)

$\sigma_x(m_y)$ stress σ_x due to virtual moment m_y, Eq. (6a)

$\sigma_{x(B)}$ stress σ_x due to bending, Eq. (8)

$\sigma_{x(D)}$ stress σ_x due to direct forces, Eq. (10)

by Kalnins [5] in 1964. Subsequently, in 1965, the solution for the response of an arbitrary shell subjected to time-dependent surface loadings was obtained by Kraus and Kalnins [6] by means of the classical method of spectral representation. The solution was expanded in terms of the modes of free vibration as determined previously by Kalnins [5], and the orthogonality of the normal modes was proved for an arbitrary shell.

In 1965, a finite element technique for the analysis of shells of revolution under both axisymmetric and asymmetric static loading was developed by Percy et al. [7] by idealizing the shell as a series of conical frusta.

In 1966, Smith [8] published his development of procedures for the static analysis of axisymmetric shell structures under axisymmetric loading by reduction of the shell to a series of ring sections. In particular, the method may be used to analyze shells with irregular meridional geometry. Explicit expressions for influence coefficients for each ring element are derived. Solutions are obtained by the flexibility method of indeterminate structural analysis. Programming of the equations developed in Ref. [8] for use in obtaining solutions on an electronic computer was accomplished by Patrick [9].

In 1966, Klein [10] also published an article describing a matrix displacement finite element approach to the linear elastic analysis of multilayer shells of revolution under axisymmetric and asymmetric dynamic and impulsive loadings. The method of solution treats the shell as a series of conical frusta joined at nodal circles.

Subsequently, Smith [11,12] published reports in which numerical procedures were given for determining the dynamic response of rotationally symmetric thin shells of revolution under time-dependent distributed impulsive and thermal loadings. The field equations consist of eight first-order partial differential equations with respect to the axis of symmetry of the shell, and the solution for each Fourier harmonic is obtained by using low-order finite difference representations for all time and spatial derivatives. Explicit relations are used to obtain displacements normal to the middle surface and along the meridians of the shell for node points inside the shell boundaries for the second and later time increments.

In 1973, Smith [13] published a report describing static solutions and stable implicit numerical solutions for the dynamic response of rotationally symmetric thin shells of revolution under time-dependent surface and thermal loadings by using a high-order finite difference representation of spatial derivatives in the system of eight first-order partial differential equations.

In 1975, Radwan and Genin [14] published their development of the equations for determining the nonlinear response of thin elastic shells of arbitrary geometry under either static or dynamic loading through the use of assumed, known, or calculated mode shape functions.

In 1977, Smith [15,16] published reports describing numerical procedures for determining the static or dynamic response of rotationally symmetric thin shells of revolution by use of both a high-order finite difference representation of the spatial derivatives and explicit relations for the dependent variables within the boundary edges of the shell for the second and succeeding time increments. The system of equations was formulated with the transverse, meridional, and circumferential displacements as the dependent variables.

In 1983, Chang et al. [17] published their development for the linear dynamic analysis of rotationally symmetric shells using finite elements and modal expansion.

In 1983, Smith [18,19] presented numerical formulations for determining both static and dynamic solutions for rotationally symmetric thin shells of revolution subjected to distributed loadings which may be discontinuous.

In 1991, Smith [20,21] completed the development of procedures for determining the total shell response of any rotationally symmetric general shell under time-dependent (or static) surface loadings by the modal superposition method.

In 1992, Heppler and Wahl [22] published their article on finite element analysis of free–free shells of revolution, which demonstrated that by use of nonconventional basis functions in the finite element method analysis the six rigid body modes are recovered as the first six modes for the case of unrestrained shells. Studies included evaluation of the vibration modes for a series of shells with both restrained and unrestrained boundaries.

In 1993, Sivadas and Ganesan [23] published their development of procedures for the dynamic analysis of rotationally symmetric circular cylindrical shells for which shell damping, shear deformation, and rotary inertia were considered in the analysis. An axisymmetric finite element representation of the shell in conjunction with a solution by the modal superposition method for either isotropic or laminated shells was used.

In 1994, Smith [24] published a second report incorporating revisions to Ref. [15], which resulted in improved numerical solutions obtained from the system of finite difference equations.

In 1995, Sinha and Mukhopadhyay [25] published their development for the dynamic analysis of stiffened plates and shells by the use of arbitrarily shaped triangular shell elements for which stiffeners may lie in any arbitrary direction within the element. The system of governing equations of motion is solved by employing the Newmark iterative method.

In 1997, Goncalves and Ramos [26] published their analysis for the free vibration of thin-walled cylindrical shells subject to homogeneous boundary conditions at each boundary of the shell. The system of equations consists of eight first-order ordinary differential equations with the four displacements and the four force variables which enter into the displacement and natural boundary conditions at each boundary of the shell as the eight fundamental variables. Variables in the circumferential direction of the shell are expanded in Fourier series.

In 1998, Meek and Wang [27] presented their analysis for the nonlinear static and dynamic response of shell structures with finite rotation. The finite element used to model the shell structure is a flat-faceted triangular shell element. An incremental iteration method in conjunction with the Newton–Raphson method is used for static analysis, while the integration scheme of Newmark is employed for dynamic analysis.

In 1998, Smith [28,29] published his analysis of shell behavior based on the use of the transverse, meridional, and circumferential displacements as the fundamental variables in the field equations. The system of equations is converted to a system of ordinary spatial finite difference equations for which a variable nodal point spacing may be used together with an ordinary finite difference representation for the time derivatives. Explicit relations are obtained for the displacements within the boundary edges of the shell for the second and later time increments. Included is the development and implementation of a numerical stability (or instability) criterion based upon an eigenvalue analysis of the explicit coefficient matrices for any selected spatial finite difference mesh and time step increment. The eigenvalues and eigenvectors of the explicit coefficient matrices are found by use of an accompanying computer program subroutine EIGNCX given and described in Ref. [30].

In 2004, Ozkul [31] published his development for the dynamic analysis of general shells by use of the finite element method. The finite element used to model the complete shell structure is a curved isoparametric eight-node trapezoidal element with five degrees of freedom per node. Hamilton's principle is used to develop the equations of motion for the shell and the Wilson-θ integration method is used for the solution of these equations. Shear deformation and rotary inertia are considered in the development.

The purpose of this article is to make available in the open literature the developed formulae for the individual ring element influence coefficients as well as the analytical procedures contained in Ref. [8] for the linear static analysis of rotationally symmetric shell structures of highly irregular geometry under axisymmetric loading. It will be seen by comparison of solutions obtained by the methods of Ref. [8] and by exact solutions of the applicable differential equations for typical plate and shell structures that the results are in very close agreement.

2. Discussion and assumptions

The equations of Ref. [8] were developed specifically to provide a needed capability to analyze the behavior of shell structures of irregular geometrical shapes not readily defined mathematically. The method of analysis is essentially the flexibility method of indeterminate structural analysis. To apply this method, the shell or plate structure has been reduced to a series of individual ring elements with a redundant radial force and a redundant shell bending moment as the unknowns at the interior faces of adjoining ring elements. It is generally assumed that force boundary conditions will be applied at the boundary edges of the reduced shell or plate structure. In the cases of displacement boundary conditions, the corresponding force boundary conditions may be readily determined by prior solution of four equations whose elements have been found by utilizing the influence coefficients for all ring elements of the complete shell or plate structure. It is assumed that there is no redundancy in the axial direction of the shell or plate structure and provision is made for prescribing zero displacement in the axial direction at either boundary of the shell or plate structure.

Total elongation of the shell or plate in the axial direction is found by summing the axial elongations for all ring elements under the prescribed loadings.

The development of the equations for the ring displacements will be made for a conical ring element of rectangular cross section (or assumed equivalent rectangular cross section) with the restriction that the meridional length of the cross section shall preferably be not greater than one and one-half times the shell element thickness. The ratio of the radius of the centroid of the ring element cross section to the ring thickness shall preferably be not less than 20. Circumferential, meridional, and shear stresses in the ring elements shall be finally determined from the actual dimensions of the ring element. Circumferential stresses in the structure shall be determined from a consideration of the stress–strain relations.

In the development, it will be assumed that the bending moment stresses in the circumferential direction for the ring elements are distributed in the same manner as they are assumed to be distributed in a straight beam section, thus neglecting the effects of curvature on the stresses. Bending and direct stresses in the plane of the cross section due to edge moments, radially applied forces, longitudinal loads, pressure loadings, and thermal effects will be assumed to vary linearly between the edges of the cross section. Deformations due to shearing stresses and direct stresses through the thickness of the ring cross section will be neglected. It will be assumed that the material is homogeneous, isotropic, and linearly elastic and that the shell structure is subjected to loadings that are statically applied.

3. Analysis for typical ring element

The geometry and the coordinate system for a typical ring element cross section are shown in Fig. 1. The orientation of the middle surface of the rectangular cross section of the ring element with respect to the axis of symmetry of the circular ring is defined by the angle α. The coordinate x is measured in the circumferential direction of the ring at the centroidal axis of the cross section. With respect to the cross section, the coordinate y is measured along the middle surface of the element from the centroidal axis and the coordinate z is measured therefrom in a direction normal to the middle surface. The coordinate y' is measured from the centroidal axis in a line parallel to the axis of symmetry of the ring element and z' is measured therefrom in a direction normal to the axis of symmetry as shown in Fig. 1.

Before proceeding with the development of the influence coefficients for a typical ring element, it is necessary to determine the circumferential stresses over the ring element cross section due to both uniformly distributed applied torques T_3 and T_4 and radially applied forces H_1 and H_2. The circumferential stresses σ_x will be expressed in terms of the y'–z' system of coordinates. However, for purposes of integration over the ring element cross section to determine the flexibility influence coefficients, the y–z system of coordinate will be used. It is thus seen that the circumferential stresses will be as determined for a coordinate system of y'–z' which has no axis of symmetry.

To aid in the development of the expressions for the forces and stresses on any ring element cross section shown in Fig. 1, plans and sections showing these forces are given in Fig. 2. Shown in Fig. 2 are a plan view of the ring element, a cross section showing the y'–z' coordinate system, and a plan view of half of a ring element showing real and virtual forces applied thereto. From the half-plan view, it is seen that, for a uniform torque T around the element, equilibrium requires that

$$M_{z'} = \int_0^{\pi/2} TR\cos\phi\,\mathrm{d}\phi = TR. \tag{1}$$

To determine $M_{y'}$, cut the structure on the diametral line $A2$–$B2$ and apply a unit virtual moment $m_{y'} = 1$ as shown in Fig. 2 before the application of the torque T. Let θ_{11} = the rotation at points $A2$ and $B2$ about the y' axis due to $m_{y'}$ = unity at $A2$ and $B2$. And let θ_{10} = the rotation at points $A2$ and $B2$ about the y' axis with $M_{y'} = 0$.

The stresses σ_x in the ring element due to $M_{z'}$ are by Eq. (132) of Ref. [32]

$$\sigma_x(M_{z'}) = \frac{M_{z'}(I_{y'}y' - I_{z'y'}z')}{I_{z'}I_{y'} - I_{z'y'}^2}. \tag{2}$$

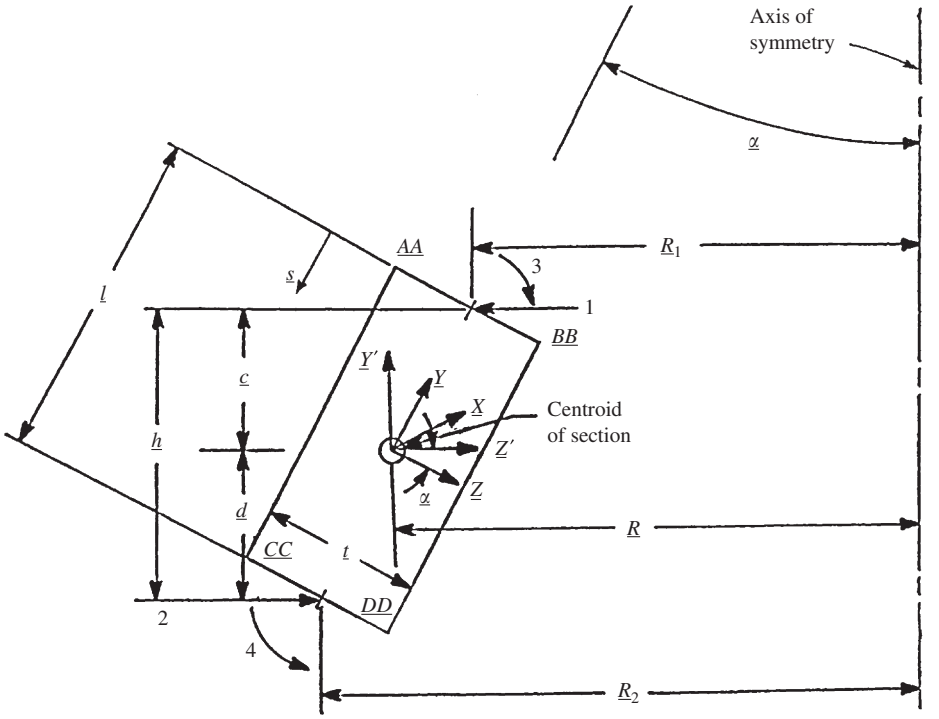

Fig. 1. Typical ring element cross section and coordinate systems. The x coordinate is measured circumferentially. AA, BB, CC, and DD are the corners of the ring element.

The stresses σ_x due to $M_{y'}$ are by Eq. (133) of Ref. [32]

$$\sigma_x(M_{y'}) = \frac{M_{y'}(I_{z'y'}y' - I_{z'}z')}{I_{z'y'} - I_{z'y'}^2}. \tag{3}$$

To facilitate the determination of θ_{11}, θ_{10}, and hence $M_{Y'}$, the substitution is made that

$$\begin{aligned} y' &= Y \\ z' &= Z. \end{aligned} \tag{4}$$

The rotation θ_{11} may be found from the relation

$$m_Y\theta_{11} = \int_0^{\pi/2}\int_A \frac{\sigma_x^2(my)\mathrm{d}A\mathrm{d}s}{E}. \tag{5a}$$

By using Eqs. (3) and (4), observing that $I_Z = \int_A Y^2\mathrm{d}A$, $I_Y = \int_A Z^2\mathrm{d}A$, and $I_{ZY} = \int_A YZ\mathrm{d}A$ and that $m_Y =$ unity, it is found that

$$\theta_{11} = \frac{\pi R I_Z}{2E(I_Z I_Y - I_{ZY}^2)}. \tag{5b}$$

The rotation θ_{10} is found from the relation

$$m_Y\theta_{10} = \int_0^{\pi/2}\int_A \frac{\sigma_x(M_Z)\sigma_x(m_Y)\,\mathrm{d}A\,\mathrm{d}s}{E}. \tag{6a}$$

By using Eqs. (2)–(4), noting that $I_Z = \int_A Y^2\,\mathrm{d}A$, $I_Y = \int_A Z^2\,\mathrm{d}A$, and $I_{ZY} = \int_A YZ\,\mathrm{d}A$, and that $m_Y =$ unity, it is seen that

$$\theta_{10} = \frac{\pi R M_Z I_{ZY}}{2E(I_Z I_Y - I_{ZY}^2)}. \tag{6b}$$

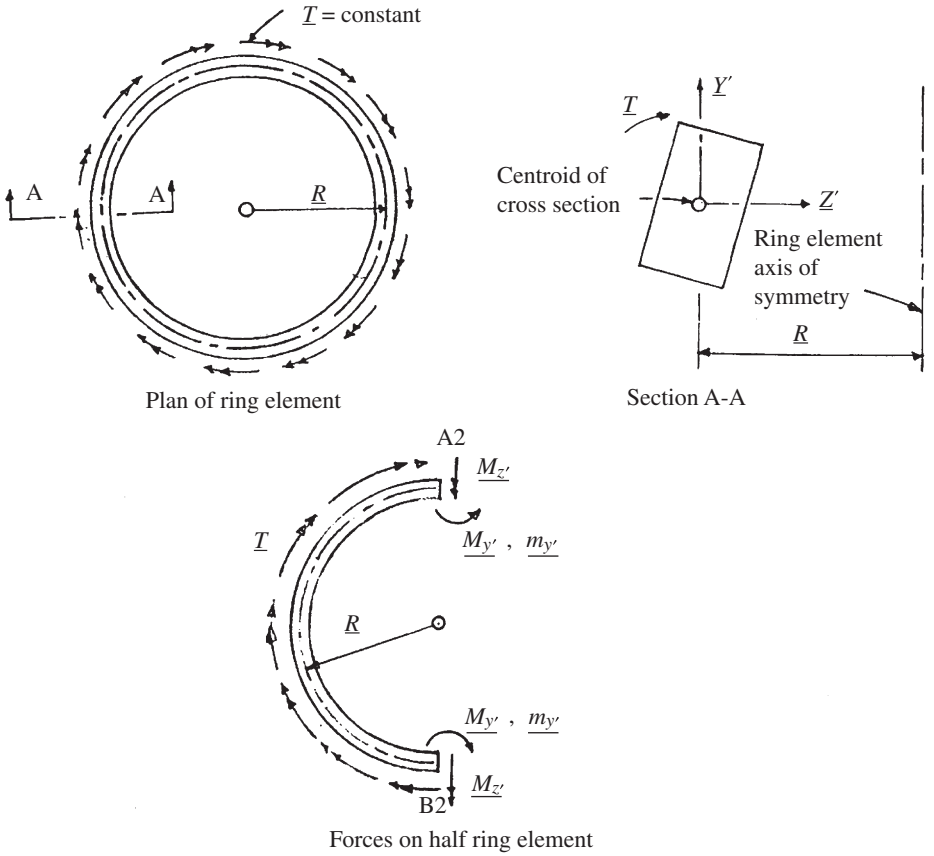

Fig. 2. Plans and sections showing forces on typical ring element. *A*2 and *B*2 are at the centroid of ring element cross section.

The value of M_Y may be found from

$$\theta_{11} M_Z + \theta_{10} = 0, \quad \text{from which} \tag{7a}$$

$$M_Y = -\frac{M_Z I_{ZY}}{I_Z}. \tag{7b}$$

The total value of σ_x developed by the torque T is given by summing the expressions in Eqs. (2) and (3), while substituting Eq. (7b) for M_Y into Eq. (3). Thus, it is found that

$$\sigma_x = \frac{M_Z Y}{I_Z}.$$

By using Eqs. (4), the equation for σ_x due to bending may be written as

$$\sigma_x(B) = \frac{M_{z'} y'}{I_{z'}}, \tag{8}$$

where $M_{z'}$ is the ring element cross-section bending moment about the z' axis and $I_{z'}$ is the moment of inertia of the ring element cross section about the z' axis.

The stresses σ_x by Eq. (8) are only those stresses due to bending of the ring element due to axisymmetric torques T_1, T_2, H_1, H_2, and other applied loadings about the centroidal axis of the element. In the case where radial forces (typically H_1) are also applied, there are developed in the ring element not only bending stresses but also direct stresses which must be added to the bending stresses. Typically, for a radial force H_1 applied at

coordinate 1 in Fig. 1, the direct circumferential force S in the ring element becomes

$$S = \int_0^{\pi/2} H_1 R \cos\phi \, \mathrm{d}\phi = H_1 R_1. \tag{9}$$

The stress σ_x in the ring element due to direct forces (typically for the H_1 application) is therefore

$$\sigma_x(D) = \frac{H_1 R_1}{A}. \tag{10}$$

In the development of the expressions for the ring element influence coefficients, both bending stresses and any developed direct stresses will be considered.

In addition to the stresses σ_x discussed immediately hereinbefore, the meridional stresses σ_y are to be considered. These are the stresses caused by the meridional bending moments M_x about the circumferential coordinate line x described in Fig. 1, by the radial forces normal to the axis of symmetry of the ring element, and by any applied or induced forces acting on the ring element. In general, for the development of the ring element influence coefficients, the forces H_1 and H_2 are assumed to be uniformly distributed across the thickness t of the element at the respective points of application, and they are zero at the opposite edge of the element. The meridional direct stresses σ_y have been assumed to vary linearly between these two edges of the element. In a similar vein, the bending stresses σ_y have been assumed to vary linearly between the element edges. The stresses σ_y due to each of the applied forces H_1, H_2, T_3, and T_4 based upon the above assumptions may be developed directly from Fig. 1, where the coordinate s shown there is given by

$$s = -y + 0.5\ell \tag{11}$$

and where the circumference of the ring element at any value of s is given by

$$b = 2\pi(R_1 + s\sin\alpha). \tag{12}$$

The stresses $\sigma_y(H_1)$ are therefore

$$\sigma_y(H_1) = -\frac{2\pi R_1 H_1 \sin\alpha(1 - s/\ell)}{bt} = -\frac{R_1 H_1 \sin\alpha(y/\ell + 0.5)}{t[R_1 + (-y + \ell/2)\sin\alpha]} \tag{13}$$

The stresses due to H_2 are

$$\sigma_y(H_2) = -\frac{(R_2 H_2 \sin\alpha)s}{t(R_1 + s\sin\alpha)\ell} = \frac{R_2 H_2 \sin\alpha(y/\ell - 0.5)}{t[R_1 + (-y + 0.5\ell)\sin\alpha]}. \tag{14}$$

The total applied circumferential bending moment due to T_3 is

$$M_x^T = 2\pi R_1 T_3(1 - s/\ell),$$

while the circumferential moment of inertia is

$$I_x^T = 2\pi(R_1 + s\sin\alpha)t^3/12,$$

where M_x^T and I_x^T are the values of M_x and I_x around the total circumference.

Hence, the bending stress σ_y is found from

$$\sigma_y(T_3) = -\frac{M_x^T z}{I_x^T} = -\frac{12R_1 T_3(1 - s/\ell)z}{(R_1 + s\sin\alpha)t^3} = -\frac{12R_1 T_3(y/\ell + 0.5)z}{[R_1 + (-y + 0.5\ell)\sin\alpha]t^3}. \tag{15}$$

The total circumferential bending moment due to T_4 is

$$M_x^T = -2\pi R_2 T_4(s/\ell).$$

Hence, the bending stress σ_y is given by

$$\sigma_y(T_4) = \frac{M_x^T z}{I_x^T} = -\frac{12R_2 T_4(s/\ell)z}{(R_1 + s\sin\alpha)t^3} = \frac{12R_2 T_4(y/\ell - 0.5)z}{[R_1 + (-y + 0.5\ell)\sin\alpha]t^3}. \tag{16}$$

It is clear from the denominators of Eqs. (13)–(16) that the stresses σ_y under given loadings at the boundaries of the ring element for values of a greater than zero are reduced as values of s are increased.

However, the values of $s\sin\alpha$ on the interval $0 \leqslant s \leqslant l$ are expected to be relatively small compared to the values of R_1, R, and R_2. Thus, it appears that the term $s\sin\alpha$ in Eqs. (13)–(16) can be neglected and that the term $(R_1 + s\sin\alpha)$ can be replaced by the average radius R at the centroid of the ring element cross section in determining the stresses σ_y to be used to determine the ring element influence coefficients. Example solutions included in this article for which solutions for both a cylindrical shell and a circular plate as obtained by the flexibility methods developed here and as obtained by solutions of the governing differential equations demonstrate that the above-described assumption of the stresses σ_y to determine the ring element influence coefficients results in an insignificant error in the final results. Definition of the stresses σ_y will therefore be given by modification of Eqs. (13)–(16) as just described above to evaluate the ring element influence coefficients.

The relations between the y' and z' system of coordinates and the y and z coordinate system are given by

$$z' = z\cos\alpha + y\sin\alpha, \tag{17a}$$

$$y' = -z\sin\alpha + y\cos\alpha. \tag{17b}$$

The displacement influence coefficients for an individual ring element will be found by first applying forces at and in the direction of coordinate 1 while all other forces are zero and calculating the displacements at and in the coordinate directions 1, 2, 3, and 4. This operation will be repeated with forces applied in turn in only the coordinate directions 2, 3, and 4, respectively. These displacements will be determined by the elastic energy theory as given by Van den Broek [33]. Basically, as applied here, we impose on the ring element an external system of virtual forces applied in the location and direction for which we desire the displacements before we apply the actual loads. This develops in the ring element a system of virtual stresses. Upon subsequent application of the actual loading, external work is done by the externally applied virtual forces acting through the external displacements caused by the actual loading. Internal work in the ring element is done by the internal virtual stresses moving through the internal strains caused by the actual loading. By equating external and internal work, we obtain our expressions for the actual external displacement at the point or line of the virtual load application.

4. Displacements of ring due to H_1

To determine the displacements $\delta_{1H_1}, \delta_{2H_1}, \delta_{3H_1}, \delta_{4H_1}$, and δ_{VH_1}, we first apply the virtual loading H_1' at and in the direction of ring coordinate 1 prior to application of the actual loading H_1, where, typically, H_1 is the radial force per unit length in the direction of coordinate 1, and where, typically, δ_{1H_1} represents the deflection in the direction of coordinate 1 due to H_1, and where, typically, H_1' is a unit virtual radial force per unit length in the direction of coordinate 1. Subsequently, we apply the actual loading H_1. The meridional stress diagram due to H_1 as shown in Fig. 3 is identical to the meridional stress diagram (not shown) due to the virtual loading H_1'. Under these loadings (and by using Eqs. (1), (8), and (10)), our actual stresses σ_x are seen to be

$$\sigma_x = \frac{H_1 R_1 c}{I_{z'}} y' + \frac{H_1 R_1}{A} = \frac{H_1 R_1 c}{I_{z'}}(y\cos\alpha - z\sin\alpha) + \frac{H_1 R_1}{A}. \tag{18a}$$

It may be seen from Fig. 3 and discussions hereinbefore relative to Eq. (13) that the stresses σ_y are represented very closely by

$$\sigma_y = -\frac{H_1 R_1 \sin\alpha}{Rt}\left(\frac{y}{\ell} + \frac{1}{2}\right), \tag{18b}$$

while the virtual stresses are

$$\sigma_{x(H_1')} = \frac{H_1' R_1 c}{I_{z'}}(y\cos\alpha - z\sin\alpha) + \frac{H_1' R_1}{A}, \tag{19a}$$

$$\sigma_{y(H_1')} = -\frac{H_1' R_1 \sin\alpha}{Rt}\left(\frac{y}{\ell} + \frac{1}{2}\right). \tag{19b}$$

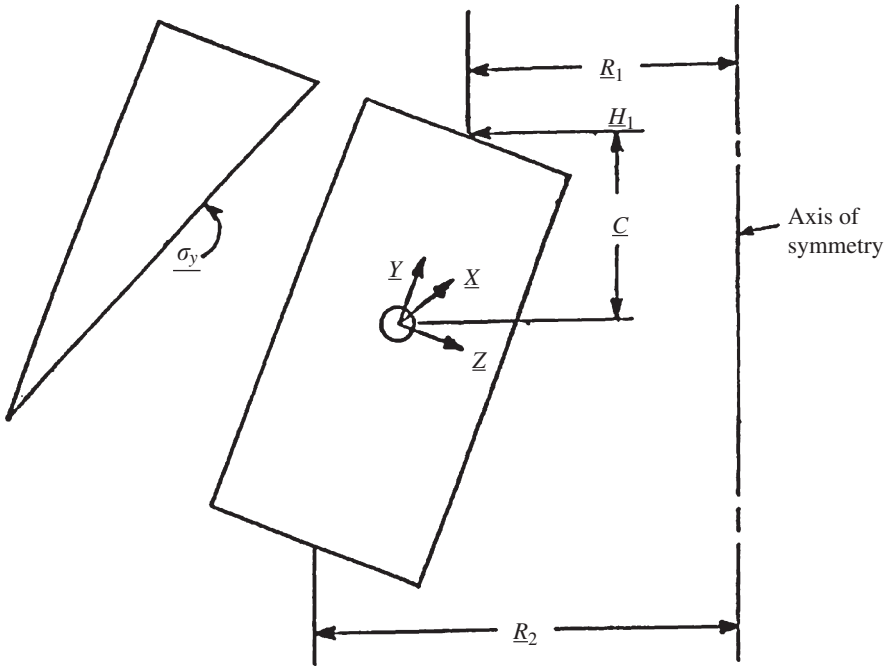

Fig. 3. Meridional stress diagram for H_1.

The actual strains are

$$\in_x(H_1) = \frac{1}{E}(\sigma_x - v\sigma_y) = \frac{H_1 R_1}{E}\left[\frac{c}{I_{z'}}(y\cos\alpha - z\sin\alpha) + \frac{1}{A} + \frac{v\sin\alpha}{Rt}\left(\frac{y}{\ell} + \frac{1}{2}\right)\right], \tag{20a}$$

$$\in_y(H_1) = \frac{1}{E}(\sigma_y - v\sigma_x) = \frac{H_1 R_1}{E}\left[-\frac{\sin\alpha}{Rt}\left(\frac{y}{\ell} + \frac{1}{2}\right) - \frac{vc}{I_{z'}}(y\cos\alpha - z\sin\alpha) - \frac{v}{A}\right]. \tag{20b}$$

By equating the external and internal work done by the above systems of actual and virtual forces, one obtains by using Eqs. (19) and (20) the expression for finding δ_{1H_1} as

$$\begin{aligned} 2\pi R_1 H_1' \delta_{1H_1} = \int_v \in(H_1)^{\sigma}(H_1')\,\mathrm{d}v = 2\pi R\Bigg\{ & \int_A \frac{H_1 R_1}{E}\left[\frac{c}{I_{z'}}(y\cos\alpha - z\sin\alpha) + \frac{1}{A} + \frac{v\sin\alpha}{Rt}\left(\frac{y}{\ell} + \frac{1}{2}\right)\right] H_1' R_1 \\ & \times\left[\frac{c}{I_{z'}}(y\cos\alpha - z\sin\alpha) + \frac{1}{A}\right]\mathrm{d}y\,\mathrm{d}z + \int_A -\frac{H_1 R_1}{E}\left[\frac{\sin\alpha}{Rt}\left(\frac{y}{\ell} + \frac{1}{2}\right) + \frac{vc}{I_{z'}}(y\cos\alpha - z\sin\alpha) + \frac{v}{A}\right] \\ & \times\left[-\frac{H_1' R_1\sin\alpha}{Rt}\left(\frac{y}{\ell} + \frac{1}{2}\right)\right]\mathrm{d}y\,\mathrm{d}z\Bigg\}. \end{aligned} \tag{21}$$

Upon performing the integrations in Eq. (21), one finds the expression for the displacement in the direction of coordinate 1 under the H_1 loading as

$$\delta_{1H_1} = \frac{H_1 R R_1}{E}\left[\frac{c^2}{I_{z'}} + \frac{1}{A} + \frac{vc\ell^2\sin\alpha\cos\alpha}{6RI_{z'}} + \frac{v\sin\alpha}{Rt} + \frac{\ell\sin^2\alpha}{3R^2 t}\right]. \tag{22}$$

To obtain our displacement at coordinate 2 due to the H_1 loading, we impose the virtual loading H'_2 at coordinate 2 prior to application of the H_1 loading. The meridional stress diagram under the H'_2 loading is shown in Fig. 4. The virtual stresses σ_x induced by the H'_2 loading are found from Eqs. (1), (8), and (10) to be

$$\sigma_x(H_2') = \frac{H_2' R_2 d}{I_{z'}}(y\cos\alpha - z\sin\alpha) - \frac{H_2' R_2}{A}. \tag{23a}$$

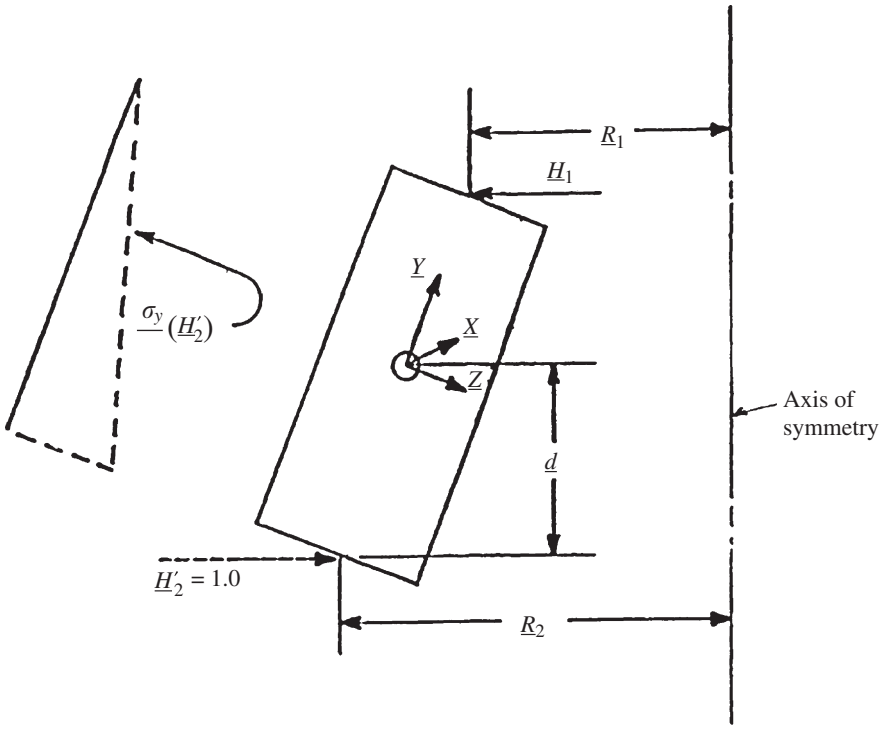

Fig. 4. Meridional stress diagram for H_2'.

It is seen from Fig. 4 and previous discussions relative to Eq. (14) that the stresses σ_y are given quite closely by

$$\sigma_y(H_2') = \frac{H_2' R_2 \sin\alpha}{Rt}\left(\frac{y}{\ell} - \frac{1}{2}\right). \tag{23b}$$

By applying the principle of virtual work, we find our expression for determining δ_{2H_1} as

$$2\pi R_2 H_2' \delta_{2H_1} = \int_v \in (H_1)\sigma(H_2')\,\mathrm{d}v. \tag{24}$$

By substituting Eqs. (20) and (23) into Eq. (24) and performing the integrations, one finds

$$\delta_{2H_1} = \frac{H_1 R R_1}{E}\left[\frac{cd}{I_{z'}} - \frac{1}{A} + \frac{\ell \sin^2\alpha}{6R^2 t}\right]. \tag{25}$$

To find the rotational displacement δ_{3H_1} due to the H_1 loading, we apply the virtual loading T_3' at and in the direction of coordinate 3 before application of the H_1 loading. The meridional moment diagram for the T_3' loading is shown in Fig. 5. The virtual meridional moment M_x' due to the T_3' loading is seen from Fig. 5 and from the previous development and discussions relative to Eq. (15) to be

$$M_x' = T_3'\left(\frac{y}{\ell} + \frac{1}{2}\right)\frac{R_1}{R}. \tag{26}$$

The virtual stresses σ_x caused by the T_3' loading are given by Eq. (8) as

$$\sigma_x(T_3') = \frac{M_{z'} y'}{I_{z'}} = -\frac{T_3' R_1}{I_{z'}}(y\cos\alpha - z\sin\alpha). \tag{27a}$$

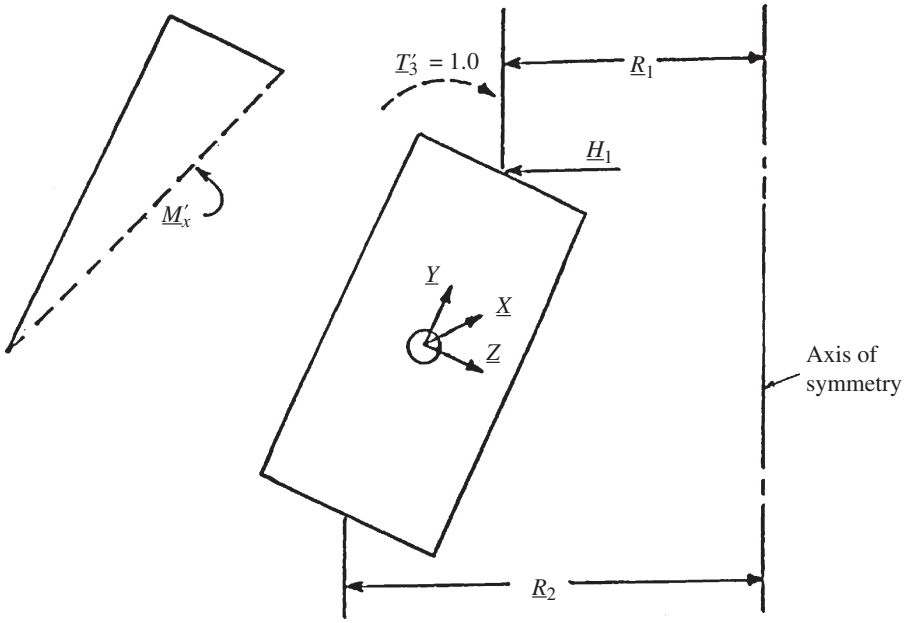

Fig. 5. Meridional moment diagram for T_3'.

The virtual stresses σ_y due to M_x' (Fig. 5) may be found from the previous development and discussions relative to Eq. (15) to be

$$\sigma_y(T_3') = -\frac{M_x' z}{I_x} = -\frac{12T_3' z}{t^3}\left(\frac{y}{\ell}+\frac{1}{2}\right)\frac{R_1}{R}. \tag{27b}$$

By invoking and applying the principle of virtual work, we find our equation for determining δ_{3H_1} to be

$$2\pi R_1 T_3' \delta_{3H_1} = \int_v \in (H_1)\sigma(T_3')\,\mathrm{d}v. \tag{28}$$

Upon substituting Eqs. (20) and (27) into Eq. (28) and performing the integrations, one finds

$$\delta_{3H_1} = -\frac{H_1 R R_1}{E I_{z'}}\left[c + \frac{v\ell^2 \sin\alpha\cos\alpha}{12R} + \frac{vc\ell\sin\alpha}{2R}\right]. \tag{29}$$

To determine the rotational displacement δ_{4H_1} caused by the H_1 loading, we apply the virtual loading T_4' at and in the direction of coordinate 4 before applying the H_1 loading. We show the meridional moment diagram for the T_4' loading in Fig. 6. The virtual meridional moment M_x' for the T_4' loading is seen from Fig. 6 and from the previous development and discussions relative to Eq. (16) to be

$$M_x' = T_4'\left(\frac{y}{\ell}-\frac{1}{2}\right)\frac{R_2}{R}. \tag{30}$$

The virtual stresses σ_x developed by the T_4' loading are found by Eq. (8) to be

$$\sigma_x T_4' = \frac{T_4' R_2}{I_{z'}}(y\cos\alpha - z\sin\alpha). \tag{31a}$$

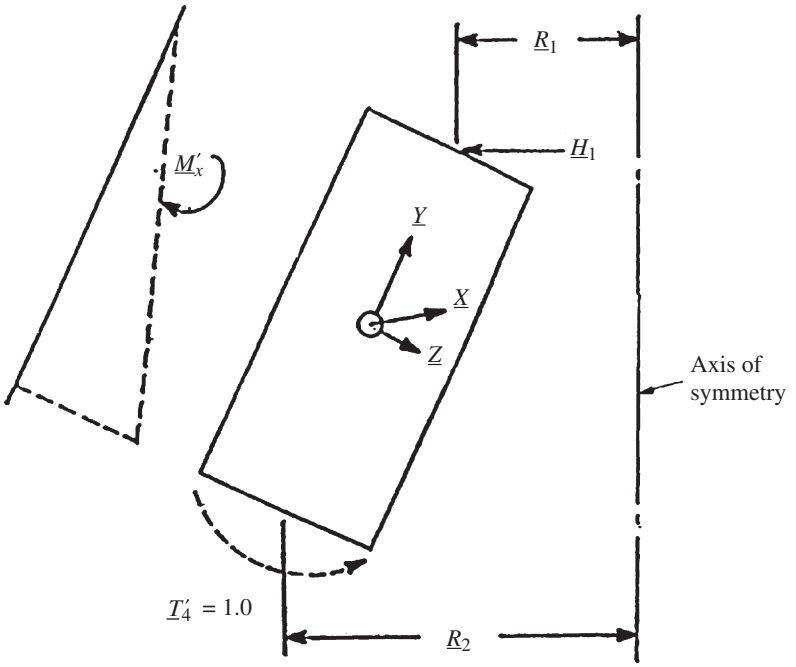

Fig. 6. Meridional moment diagram for T'_4.

The virtual stresses due to M'_x (Fig. 6) may be found from the previous development and discussions relative to Eq. (16) to be

$$\sigma_{y(T'_4)} = \frac{12T'_4 z}{t^3}\left(\frac{y}{\ell} - \frac{1}{2}\right)\frac{R_2}{R}. \tag{31b}$$

Upon application of the principle of virtual work, we obtain our expression for finding δ_{4H_1} to be

$$2\pi R_2 T'_4 \delta_{4H_1} = \int_v \in (H_1)\sigma(T'_4)\,\mathrm{d}v. \tag{32}$$

By substitution of Eqs. (20) and (31) into Eq. (32) and performing the integrations, one finds the equation for δ_{4H_1} to be

$$\delta_{4H_1} = \frac{H_1 R R_1}{EI_{z'}}\left[c + \frac{v\ell^2 \sin\alpha\cos\alpha}{12R} - \frac{vc\ell\sin\alpha}{2R}\right]. \tag{33}$$

To determine the change in length of the ring element in the direction of the axis of symmetry due to H_1, we apply parallel to the axis of symmetry of the ring (before application of the real loading H_1) the virtual loading $F'_1 = 1.0$ lb per unit length in the circumferential direction of the ring as shown in Fig. 7. The virtual stresses σ_x are found by use of Eqs. (1) and (8) to be

$$\sigma_x(F'_1) = \frac{F'_1 R_1(R_z - R_1)}{I_{z'}}[y\cos\alpha - z\sin\alpha]. \tag{34a}$$

In accordance with the development and discussion of Eqs. (13)–(16), the virtual stresses σ_y will be assumed to be given by

$$\sigma_y(F'_1) = \frac{F'_1 R_1 \cos\alpha}{Rt}. \tag{34b}$$

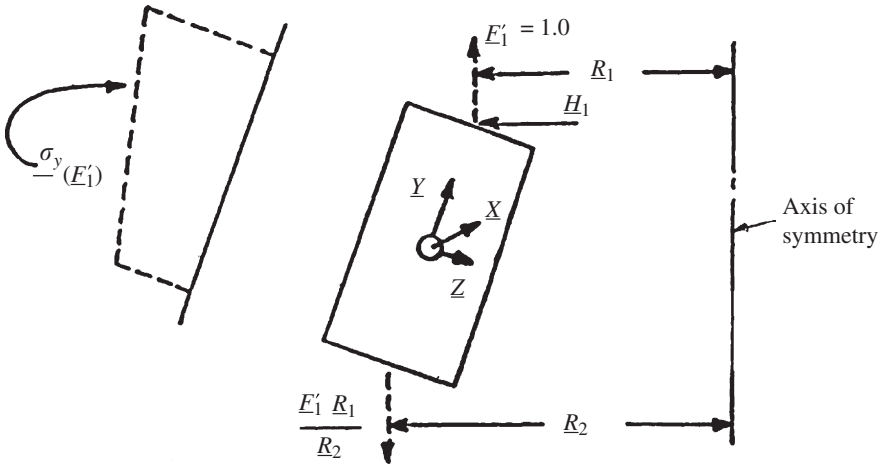

Fig. 7. Meridional stress diagram for F'_1.

By invoking and applying the principle of virtual work, we find our equation for determining δ_{VH_1} to be

$$2\pi R_1 F'_1 \delta_{VH_1} = \int_v \in (H_1)\sigma(F'_1)\,\mathrm{d}v. \tag{35}$$

By substitution of Eqs. (20) and (34) into Eq. (35) and performing the integrations, one finds the expression for axial change in length of the ring element due to H_1 to be

$$\delta_{VH_1} = \frac{H_1 R R_1}{E}\left[\frac{c(R_2 - R_1)}{I_{z'}} + \frac{v\ell^2(R_2 - R_1)\sin\alpha\cos\alpha}{12RI_{z'}} - \frac{\ell\sin\alpha\cos\alpha}{2R^2t} - \frac{v\cos\alpha}{Rt}\right]. \tag{36}$$

5. Displacements of ring due to H_2

In a manner similar to that used to develop the equations for deformations due to H_1, the following equations, which are based upon the application of H_2 as the actual loading, are obtained for the deformations due to H_2:

$$\delta_{1H_2} = \frac{H_2 R R_2}{E}\left[\frac{cd}{I_{z'}} - \frac{1}{A} + \frac{\ell\sin^2\alpha}{6R^2t}\right] \tag{37}$$

$$\delta_{2H_2} = \frac{H_2 R R_2}{E}\left[\frac{d^2}{I_{z'}} + \frac{1}{A} - \frac{vd\ell^2\sin\alpha\cos\alpha}{6RI_{z'}} + \frac{\ell\sin^2\alpha}{3R^2t} - \frac{v\sin\alpha}{Rt}\right]. \tag{38}$$

$$\delta_{3H_2} = \frac{H_2 R R_2}{EI_{z'}}\left[-d + \frac{v\ell^2\sin\alpha\cos\alpha}{12R} - \frac{vd\ell\sin\alpha}{2R}\right] \tag{39}$$

$$\delta_{4H_2} = \frac{H_2 R R_2}{EI_{z'}}\left[d - \frac{v\ell^2\sin\alpha\cos\alpha}{12R} - \frac{vd\ell\sin\alpha}{2R}\right] \tag{40}$$

$$\delta_{VH_2} = \frac{H_2 R R_2}{E}\left[\frac{d(R_2 - R_1)}{I_{z'}} - \frac{v\ell^2(R_2 - R_1)\sin\alpha\cos\alpha}{12RI_{z'}} - \frac{\ell\sin\alpha\cos\alpha}{2R^2t} + \frac{v\cos\alpha}{Rt}\right]. \tag{41}$$

6. Displacements of ring due to T_3

To derive the equations for deformations due to the actual loading T_3, we proceed in the same manner outlined above in detail for the H_1 loading and find our equations for the displacements due to the T_3 loading to be

$$\delta_{1T_3} = -\frac{T_3 R R_1}{EI_{z'}}\left[c + \frac{v\ell^2 \sin\alpha\cos\alpha}{12R} + \frac{vc\ell\sin\alpha}{2R}\right] \tag{42}$$

$$\delta_{2T_3} = \frac{T_3 R R_1}{EI_{z'}}\left[-d + \frac{v\ell^2 \sin\alpha\cos\alpha}{12R} - \frac{vd\ell\sin\alpha}{2R}\right] \tag{43}$$

$$\delta_{3T_3} = \frac{T_3 R R_1}{EI_{z'}} + \frac{vT_3 R_1 \ell\sin\alpha}{EI_{z'}} + \frac{4T_3 R_1 \ell}{ERt^3} \tag{44}$$

$$\delta_{4T_3} = -\frac{T_3 R R_1}{EI_{z'}} + \frac{2T_3 R_1 \ell}{ERt^3} \tag{45}$$

$$\delta_{VT_3} = -\frac{T_3 R R_1 (R_2 - R_1)}{EI_{z'}}\left[1 + \frac{v\ell\sin\alpha}{2R}\right]. \tag{46}$$

7. Displacements of ring due to T_4

By proceeding in a manner similar to that used to find the equations for the H_1 loading, we obtain the following equations for the ring coordinate displacements due to the T_4 loading:

$$\delta_{1T_4} = \frac{T_4 R R_2}{EI_{z'}}\left[c + \frac{v\ell^2 \sin\alpha\cos\alpha}{12R} - \frac{vc\ell\sin\alpha}{2R}\right] \tag{47}$$

$$\delta_{2T_4} = \frac{T_4 R R_2}{EI_{z'}}\left[d - \frac{v\ell^2 \sin\alpha\cos\alpha}{12R} - \frac{vd\ell\sin\alpha}{2R}\right] \tag{48}$$

$$\delta_{3T_4} = -\frac{T_4 R R_2}{EI_{z'}} + \frac{2T_4 R_2 \ell}{ERt^3} \tag{49}$$

$$\delta_{4T_4} = \frac{T_4 R R_2}{EI_{z'}} - \frac{vT_4 R_2 \ell\sin\alpha}{EI_{z'}} + \frac{4T_4 R_2 \ell}{ERt^3} \tag{50}$$

$$\delta_{VT_4} = \frac{T_4 R R_2 (R_2 - R_1)}{EI_{z'}}\left[1 - \frac{v\ell\sin\alpha}{2R}\right]. \tag{51}$$

8. Loadings on free ring element due to uniform pressure with element restrained axially at R_2

We assume for each individual ring element that the applied pressure loading is uniform and acts at the ring element middle surface and that axial restraint against motion is developed at the edge of the ring associated with the radius R_2 as shown in Fig. 8. For purposes of analysis, we replace the pressure loading by its components H_p applied radially and V_p applied normal thereto at the center of pressure as shown also in Fig. 8.

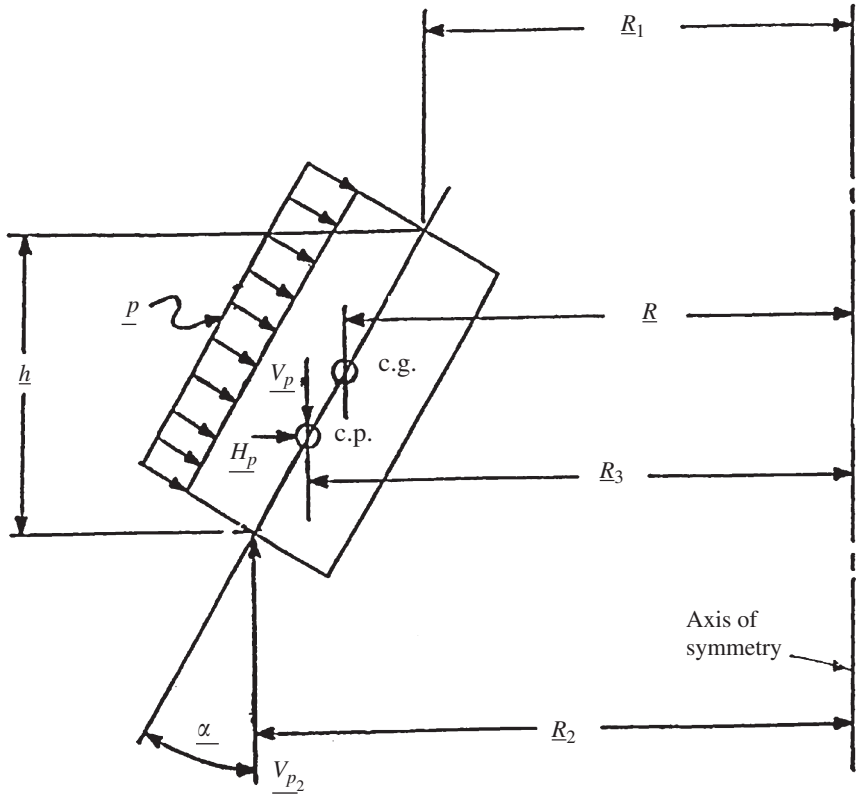

Fig. 8. Forces on ring element with axial restraint at R_2.

The area of the middle surface of the ring element is given by

$$G = \pi(R_1 + R_2)\sqrt{(R_2 - R_1)^2 + h^2}. \tag{52}$$

The loadings H_p and V_p applied at the center of pressure are given by

$$H_p = \frac{Gp\cos\alpha}{2\pi R_3} = \frac{ph(R_1 + R_2)}{2R_3}, \tag{53a}$$

$$V_p = \frac{Gp\sin\alpha}{2\pi R_3} = \frac{p(R_2^2 - R_1^2)}{2R_3}, \tag{53b}$$

where H_p and V_p are the assumed equivalent uniform line loadings at the center of pressure due to the pressure loading p as shown in Fig. 8, and where R_3 is given by

$$R_3 = \frac{2(R_2^3 - R_1^3)}{3(R_2^2 - R_1^2)} \quad (R_1 \neq R_2), \tag{54a}$$

$$R_3 = 0.5(R_1 + R_2) \quad (R_1 = R_2). \tag{54b}$$

The loading V_{p2} developed at the edge of the ring element defined by the radius R_2 in Fig. 8 is

$$V_{p2} = \frac{Gp\sin\alpha}{2\pi R_2} = \frac{p(R_2^2 - R_1^2)}{2R_2}. \tag{55}$$

The torque T_p per unit length about the centroidal axis of the cross section of the ring element due to the pressure loading p, considered positive for a clockwise rotation of the cross section as shown in Fig. 8, may be determined by consideration of the forces acting thereon in Fig. 8.

This development will be clarified if the terms H_p^T and V_p^T are defined as the radial and longitudinal loads, respectively, around the total circumference of the ring element and note that

$$\cos\alpha = h/[(R_2 - R_1)^2 + h^2]^{1/2}, \tag{56a}$$

$$\sin\alpha = (R_2 - R_1)/[(R_2 - R_1)^2 + h^2]^{1/2}, \tag{56b}$$

$$\cot\alpha = h/(R_2 - R_1). \tag{56c}$$

Thus, from Eqs. (53a) and (53b), respectively, we find

$$H_p^T = 2\pi R_3 H_p = \pi p h(R_1 + R_2), \tag{57a}$$

$$V_p^T = 2\pi R_3 V_p = \pi p(R_2^2 - R_1^2). \tag{57b}$$

Hence,

$$\begin{aligned} T_p^T &= V_p^T(R_2 - R_3) - H_p^T(R_3 - R)\cot\alpha \\ &= \pi p[(R_2^2 - R_1^2)(R_2 - R_3) - h^2(R_1 + R_2)(R_3 - R)/(R_2 - R_1)] \end{aligned}$$

and $T_p = T_p^T/2\pi R$, resulting in

$$T_p = \frac{p[(R_2^2 - R_1^2)(R_2 - R_3)}{2R} - \frac{ph^2(R_1 + R_2)(R_3 - R)}{2R(R_2 - R_1)}. \tag{58}$$

9. Torque on free ring element due to axial loadings

In addition to pressure loadings on the shell structure, which have been considered previously, we make provision for the application of loads in the direction of the axis of symmetry. Thus, we require an analysis of the deformation of each individual ring element under these axial loadings. The loadings to be considered for any ring element are shown in Fig. 9. These loadings induce a torque T_L on the ring, where T_L is the torque per unit length of circumference measured at the centroidal axis of the ring element. It may be seen from Fig. 9 that the total circumferential load applied at the location of R_1 is

$$L^T = 2\pi R_1 L.$$

The total circumferential load applied at the location of R_2 is also

$$L^T = 2\pi R_2(LR_1/R_2).$$

These two opposing and equal longitudinal forces develop the torque

$$T_L^T = 2\pi R_1 L(R_2 - R_1)$$

and a value of

$$T_L = LR_1(R_2 - R_1)/R. \tag{59}$$

10. Total torque on free ring element due to external loadings with axial restraint at R_2

With axial restraint provided at the edge of the ring element associated with the radius R_2, we obtain the torque due to combined pressure loadings and axial loadings by combining the results from Eqs. (58) and

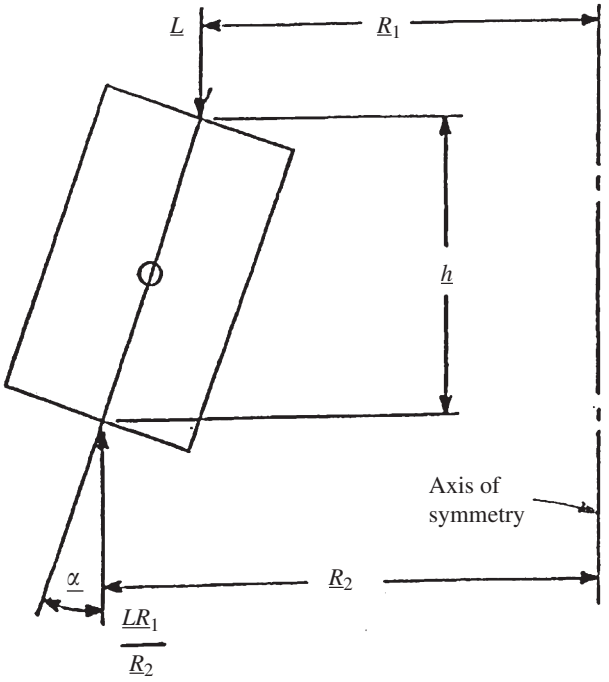

Fig. 9. Axial forces on ring.

(59) to find

$$T_{02} = T_p + T_L = \frac{p(R_2^2 - R_1^2)(R_2 - R_3)}{2R} - \frac{ph^2(R_1 + R_2)(R_3 - R)}{2R(R_2 - R_1)} + \frac{LR_1(R_2 - R_1)}{R}, \tag{60}$$

where the torque T_{02} is based upon longitudinal restraint at R_2.

11. Free ring element displacements due to temperature changes

In our analysis of any shell structure, we make provision for axisymmetric temperature changes throughout the complete structure. These changes may vary from ring element to ring element throughout the entire structure. However, we assume that the temperature change Q is constant throughout any single ring element. We further assume, as tacitly already assumed hereinbefore, that the temperature changes are of such magnitude that Young's modulus E and Poisson's ratio v may be assumed to be constant. Our displacements in the coordinate directions 1, 2, 3, and 4 and in the axial direction for any particular ring element will be given by

$$\delta_{1T} = \beta Q R_1, \tag{61a}$$

$$\delta_{2T} = -\beta Q R_2, \tag{61b}$$

$$\delta_{3T} = \frac{\beta Q(R_2 - R_1)\cos\alpha}{\ell}, \tag{61c}$$

$$\delta_{4T} = \frac{-\beta Q(R_2 - R_1)\cos\alpha}{\ell}, \tag{61d}$$

$$\delta_{VT} = \beta Q h, \tag{61e}$$

where β is the coefficient of thermal expansion, and where Q is the ring temperature rise.

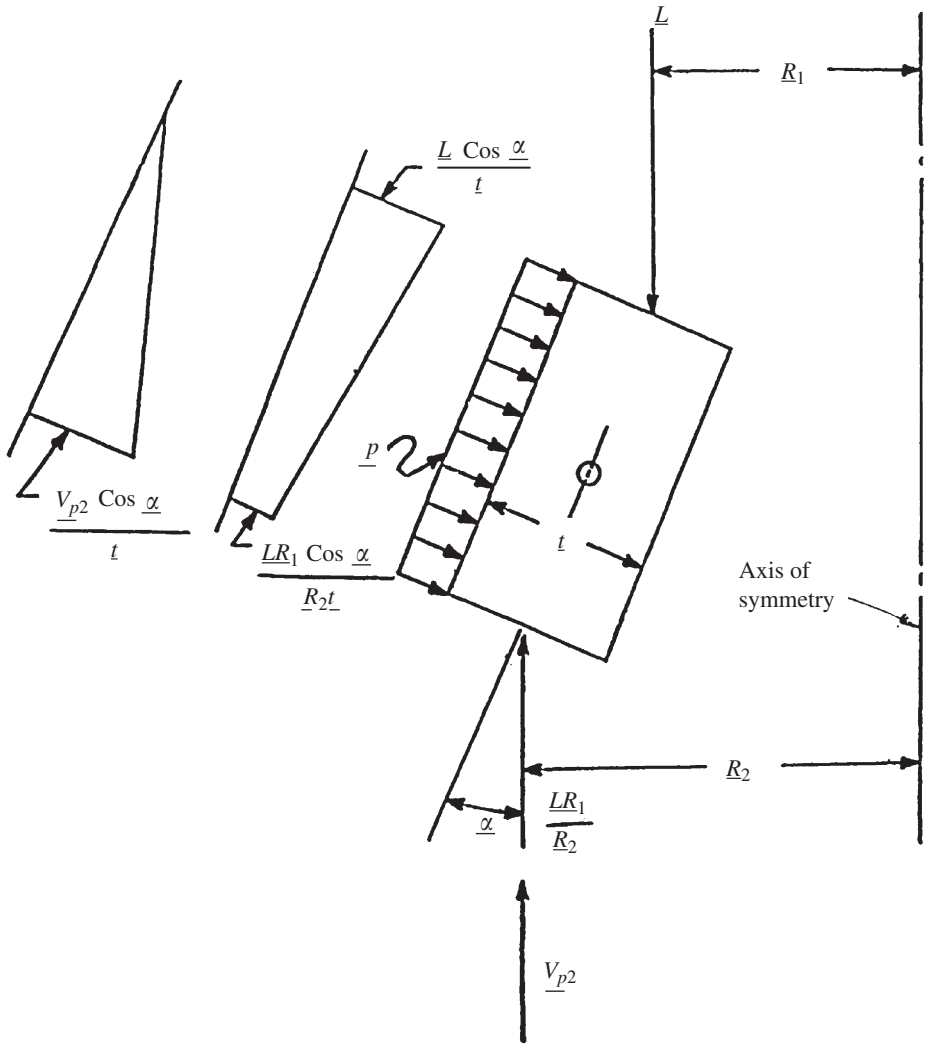

Fig. 10. Loading and meridional stress assumptions with axial restraint at R_2.

12. Free ring element displacements due to pressure and axial loadings with axial restraint at R_2

Our displacements for the coordinate directions 1, 2, 3, and 4 and in the axial direction for a typical free ring element due to pressure loadings and known axial loadings will be obtained by using the principle of virtual work as used previously to obtain the ring element influence coefficients. The loadings and meridional stress diagrams associated with these loadings are shown in Fig. 10. Our stresses σ_x under these loadings are found by use of Eqs. (1), (8), and (10) to be

$$\sigma_x = -\frac{T_{02}R}{I_{z'}}(y\cos\alpha - z\sin\alpha) - \frac{H_p R_3}{A}. \tag{62a}$$

It may be seen from Fig. 10 that under the loadings L the stresses σ_y vary only slightly with y. We therefore assume them to be the average value at the centroid of the ring element cross section. In the case of the boundary loading V_{p2}, which is a triangular shaped loading, it is assumed, in accordance with the development and discussions relative to Eqs. (13)–(16) hereinbefore, that the values of σ_y will be found closely on the basis of the value of R at the centroid of the ring element cross-section, with R assumed to be constant between the

ring element boundaries. We therefore assume σ_x to be given by

$$\sigma_y = -\left(\frac{L\cos\alpha}{t}\right)\frac{R_1}{R} + \frac{V_{p2}\cos\alpha}{t}\left(\frac{R_2}{R}\right)\left(\frac{y}{\ell}-\frac{1}{2}\right). \tag{62b}$$

The accompanying strains are

$$\in_x = \frac{1}{E}(\sigma_x - v\sigma_y) = -\frac{T_{02}R}{EI_{z'}}(y\cos\alpha - z\sin\alpha) - \frac{H_pR_3}{EA} + \frac{v}{E}\left[+\frac{LR_1\cos\alpha}{Rt} - \frac{V_{p2}R_2\cos\alpha}{Rt}\left(\frac{y}{\ell}-\frac{1}{2}\right)\right], \tag{63a}$$

$$\in_y = \frac{1}{E}(\sigma_y - v\sigma_x) = \frac{1}{E}\left[-\frac{LR_1\cos\alpha}{Rt} + \frac{V_{p2}R_2\cos\alpha}{Rt}\left(\frac{y}{\ell}-\frac{1}{2}\right)\right] + \frac{vT_{02}R}{EI_{z'}}(y\cos\alpha - z\sin\alpha) - \frac{vH_pR_3}{EA}. \tag{63b}$$

By applying the principle of virtual work, we have the following equations for obtaining the free ring displacements due to pressure and axial loadings for the case of axial restraint at the edge of the ring associated with the radius R_2:

$$2\pi R_1 H'_1\delta_{10} = \int_v \in_{(0)}\sigma(H'_1)\,\mathrm{d}v, \tag{64}$$

$$2\pi R_2 H'_2\delta_{20} = \int_v \in_{(0)}\sigma(H'_2)\,\mathrm{d}v, \tag{65}$$

$$2\pi R_1 T'_3\delta_{30} = \int_v \in_{(0)}\sigma(T'_3)\,\mathrm{d}v, \tag{66}$$

$$2\pi R_2 T'_4\delta_{40} = \int_v \in_{(0)}\sigma(T'_4)\,\mathrm{d}v, \tag{67}$$

$$2\pi R_1 F'_1\delta_{V0} = \int_v \in_{(0)}\sigma(F'_1)\,\mathrm{d}v. \tag{68}$$

In Eqs. (64)–(68), the stresses due to H'_1, H'_2, T'_3, T'_4, and F'_x are given respectively by Eqs. (19), (23), (27), (31), and (34). The strains $\in_{(0)}$ are given by Eqs. (63) as $\in_x$ and $\in_y$. By making appropriate substitutions of Eqs. (19), (23), (27), (31), (34), and (63) into Eqs. (64)–(68) and performing the indicated integrations, the desired displacements δ_{10}, δ_{20}, δ_{30}, δ_{40}, and δ_{V0} are found to be

$$\delta_{10} = \left\{-\frac{T_{02}R^2c}{EI_{z'}} - \frac{H_pRR_3}{EA} - \frac{vV_{p2}R_2c\ell^2\cos^2\alpha}{12EI_{z'}} + \frac{v\cos\alpha}{2Et}(2LR_1 + V_{p2}R_2)\right\} + \left\{\frac{-vT_{02}R\ell^2\sin\alpha\cos\alpha}{12EI_{z'}} - \frac{vH_pR_3\sin\alpha}{2Et} + \frac{\ell\sin\alpha\cos\alpha}{6EtR}(3LR_1 + V_{p2}R_2)\right\}, \tag{69}$$

$$\delta_{20} = -\left\{\frac{T_{02}R^2d}{EI_{z'}} - \frac{H_pRR_3}{EA} + \frac{vV_{p2}R_2\,d\ell^2\cos^2\alpha}{12EI_{z'}} + \frac{v\cos\alpha}{2Et}(2LR_1 + V_{p2}R_2)\right\} - \left\{\frac{-vT_{02}R\ell^2\sin\alpha\cos\alpha}{12EI_{z'}} + \frac{vH_pR_3\sin\alpha}{2Et} - \frac{\ell\sin\alpha\cos\alpha}{6EtR}(3LR_1 + V_{p2}R_2)\right\}, \tag{70}$$

$$\delta_{30} = T_{02}\left[\frac{R^2}{EI_{z'}} + \frac{vR\ell\sin\alpha}{2EI_{z'}}\right] + \frac{vV_{p2}R_2\ell^2\cos^2\alpha}{12EI_{z'}}, \tag{71}$$

$$\delta_{40} = -T_{02}\left[\frac{R^2}{EI_{z'}} - \frac{vR\ell\sin\alpha}{2EI_{z'}}\right] - \frac{vV_{p2}R_2\ell^2\cos^2\alpha}{12EI_{z'}}, \tag{72}$$

$$\delta_{V0} = -\frac{T_{02}R^2(R_2-R_1)}{EI_{z'}} - \frac{vV_{p2}(R_2-R_1)R_2\ell^2\cos^2\alpha}{12EI_{z'}} - \frac{\ell\cos^2\alpha}{2ERt}(2LR_1 + V_{p2}R_2) + \frac{vH_pR_3\cos\alpha}{Et}. \tag{73}$$

13. Free ring element displacements due to combined pressure, axial loads, and thermal effects with axial restraint at R_2

Our complete shell structure will be composed of a number of ring elements extending in the meridional direction of the shell from one boundary to the opposite boundary. We assume that one boundary edge of the shell is that edge located at coordinates 1 and 3 as shown in Fig. 1 and that a radial force H_{B1} at coordinate 1 and a shell bending moment T_{B3} at coordinate 3 may be applied as force boundary conditions at that boundary. For the opposite boundary edge of the shell, we assume the boundary edge located at coordinates 2 and 4 as shown in Fig. 1 to constitute that boundary and that a radial force H_{B2} at coordinate 2 and a shell bending moment T_{B4} at coordinate 4 may be applied as force boundary conditions at this opposite boundary. We designate the first above-described boundary element as element 1. The second described boundary element will be designated as element N, where N is the total number of ring elements in the complete shell structure. For the boundary element 1, our free ring displacements will be given by

$$\Delta_{10} = \delta_{10} + \delta_{1T} + H_{B1}\delta_{1H_1''} + T_{B3}\delta_{1T_3''}, \tag{74a}$$

$$\Delta_{20} = \delta_{20} + \delta_{2T} + H_{B1}\delta_{2H_1''} + T_{B3}\delta_{2T_3''}, \tag{74b}$$

$$\Delta_{30} = \delta_{30} + \delta_{3T} + H_{B1}\delta_{3H_1''} + T_{B3}\delta_{3T_3''}, \tag{74c}$$

$$\Delta_{40} = \delta_{40} + \delta_{4T} + H_{B1}\delta_{4H_1''} + T_{B3}\delta_{4T_3''}, \tag{74d}$$

$$\Delta_{V0} = \delta_{V0} + \delta_{VT} + H_{B1}\delta_{VH_1''} + T_{B3}\delta_{VT_3''}, \tag{74e}$$

where the double primes on H_1 and T_3 denote unit values per unit of circumferential length.

For ring elements 2 through $N-1$, our free ring displacements will be

$$\Delta_{10} = \delta_{10} + \delta_{1T}, \tag{75a}$$

$$\Delta_{20} = \delta_{20} + \delta_{2T}, \tag{75b}$$

$$\Delta_{30} = \delta_{30} + \delta_{3T}, \tag{75c}$$

$$\Delta_{40} = \delta_{40} + \delta_{4T}, \tag{75d}$$

$$\Delta_{V0} = \delta_{V0} + \delta_{VT}. \tag{75e}$$

For ring element N, we have

$$\Delta_{10} = \delta_{10} + \delta_{1T} + H_{B2}\delta_{1H_2''} + T_{B4}\delta_{1T_4''}, \tag{76a}$$

$$\Delta_{20} = \delta_{20} + \delta_{2T} + H_{B2}\delta_{2H_2''} + T_{B4}\delta_{2T_4''}, \tag{76b}$$

$$\Delta_{30} = \delta_{30} + \delta_{3T} + H_{B2}\delta_{3H_2''} + T_{B4}\delta_{3T_4''}, \tag{76c}$$

$$\Delta_{40} = \delta_{40} + \delta_{4T} + H_{B2}\delta_{4H_2''} + T_{B4}\delta_{4T_4''}, \tag{76d}$$

$$\Delta_{V0} = \delta_{V0} + \delta_{VT} + H_{B2}\delta_{VH_2''} + T_{B4}\delta_{VT_4''}, \tag{76e}$$

where the double primes on H_2 and T_4 denote unit values per unit of circumferential length.

14. Free ring element displacements due to pressure and axial loadings with axial restraint at R_1

The loadings and meridional stress diagrams for pressure and axial forces with axial restraint of the ring element at the edge of the ring associated with the radius R_1 are shown in Fig. 11.

The force V_{p1} shown in Fig. 11 is given by

$$V_{p1} = \frac{p(R_2^2 - R_1^2)}{2R_1}. \tag{77}$$

By using Eqs. (57) to define ${H_p}^T$ and ${V_p}^T$ and considering only the forces due to the pressure loading p in Fig. 11, the torque T_p, considered positive for clockwise rotation of the cross section, is found to be

$$T_p^T = V_p^T(R_1 - R_3) - H_p^T(R_3 - R)\cot\alpha = p[(R_2^2 - R_1^2)(R_1 - R_3) - h^2(R_1 + R_2)(R_3 - R)/(R_2 - R_1).$$

Thus, $T_p = T_p^T/2\pi R$, resulting in

$$T_p = \frac{p(R_2^2 - R_1^2)(R_1 - R_3)}{2R} - \frac{ph^2(R_1 + R_2)(R_3 - R)}{2R(R_2 - R_1)}, \tag{78}$$

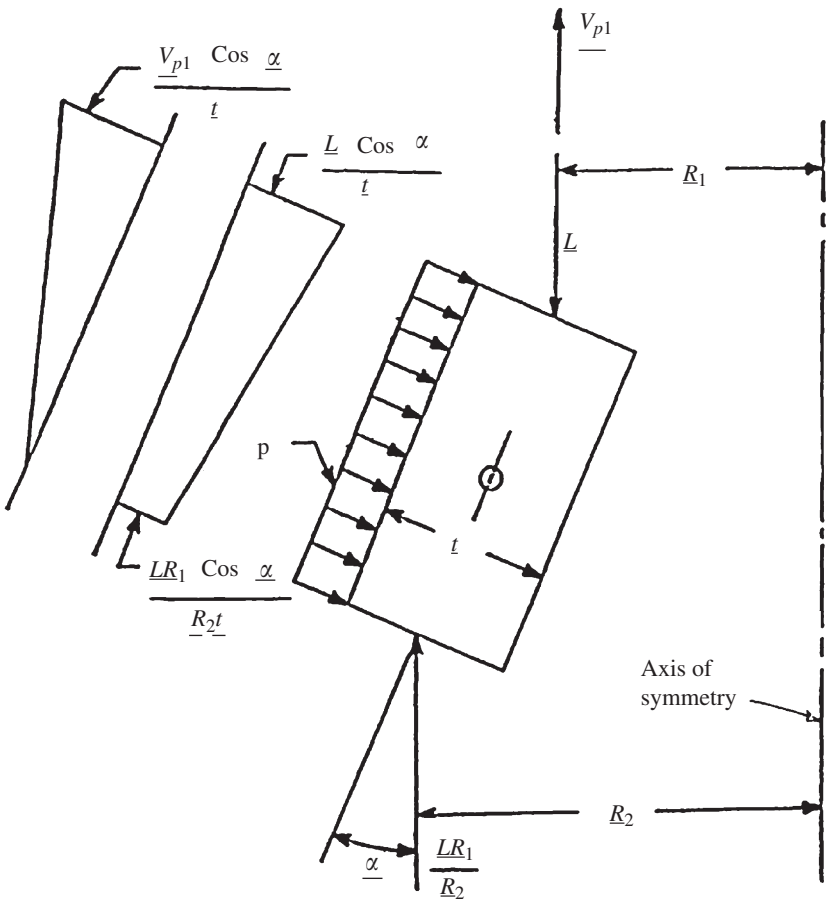

Fig. 11. Loading and meridional stress assumptions with axial restraint at R_1.

and the total torque T_{01} due to combined pressure loadings p and axial load L, by using Eq. (59), is found to be

$$T_{01} = T_p + T_L = \frac{p(R_2^2 - R_1^2)(R_1 - R_3)}{2R} - \frac{ph^2(R_1 + R_2)(R_3 - R)}{2R(R_2 - R_1)} + \frac{LR_1(R_2 - R_1)}{R}. \tag{79}$$

By using the definitions for V_{p1} by Eq. (77), T_{01} by Eq. (79), and H_p by Eq. (53a), and proceeding in the same manner as used to find the free ring displacements with axial restraint at R_2, we find the displacements δ_{10}, δ_{20}, δ_{30}, δ_{40}, and δ_{V0} under pressure and axial loadings with axial restraint at R_1 to be

$$\delta_{10} = \left\{ -\frac{T_{01}R^2 c}{EI_{z'}} - \frac{H_p R R_3}{EA} - \frac{\nu V_{p1} R_1 c \ell^2 \cos^2\alpha}{12EI_{z'}} + \frac{\nu \cos\alpha}{2Et}(2LR_1 - V_{p1}R_1) \right\} + \left\{ -\frac{\nu T_{01} R \ell^2 \sin\alpha \cos\alpha}{12EI_{z'}} - \frac{\nu H_p R_3 \sin\alpha}{2Et} + \frac{\ell \sin\alpha \cos\alpha}{6EtR}(3LR_1 - 2V_{p1}R_1) \right\}, \tag{80}$$

$$\delta_{20} = -\left\{ \frac{T_{01}R^2 d}{EI_{z'}} - \frac{H_p R R_3}{EA} + \frac{\nu V_{p1} R_1 d \ell^2 \cos^2\alpha}{12EI_{z'}} + \frac{\nu \cos\alpha}{2Et}(2LR_1 - V_{p1}R_1) \right\} - \left\{ \frac{-\nu T_{01} R \ell^2 \sin\alpha \cos\alpha}{12EI_{z'}} + \frac{\nu H_p R_3 \sin\alpha}{2Et} - \frac{\ell \sin\alpha \cos\alpha}{6EtR}(3LR_1 - V_{p1}R_1) \right\}, \tag{81}$$

$$\delta_{30} = T_{01}\left[\frac{R^2}{EI_{z'}} + \frac{\nu R \ell \sin\alpha}{2EI_{z'}} \right] + \frac{\nu V_{p1} R_1 \ell^2 \cos^2\alpha}{12EI_{z'}}, \tag{82}$$

$$\delta_{40} = -T_{01}\left[\frac{R^2}{EI_{z'}} - \frac{\nu R \ell \sin\alpha}{2EI_{z'}} \right] - \frac{\nu V_{p1} R_1 \ell^2 \cos^2\alpha}{12EI_{z'}}, \tag{83}$$

$$\delta_{V0} = -\frac{T_{01}R^2(R_2 - R_1)}{EI_{z'}} - \frac{\nu V_{p1}(R_2 - R_1) R_1 \ell^2 \cos^2\alpha}{12EI_{z'}} - \frac{\ell \cos^2\alpha}{2ERT}(2LR_1 - V_{p1}R_1) + \frac{\nu H_p R_3 \cos\alpha}{Et}. \tag{84}$$

By using Eqs. (80)–(84) in lieu of Eqs. (69)–(73) for free ring displacements under combined pressure and axial loadings with axial restraint at R_1, one will find the total free ring displacements as given already in Eqs. (74)–(76).

15. Formulation of procedure for analysis of axisymmetric shells under axisymmetric loadings

We show a typical shell structure and loading in Fig. 12. The boundary forces H_{B1}, T_{B3}, H_{B2}, and T_{B4} represent prescribed boundary forces per unit circumferential length at each boundary. The thickness of the shell and the applied pressure loading p may vary along the shell meridian.

The analysis will be performed by the standard flexibility method of indeterminate structural analysis. Our matrix form of the continuity equations for this solution is

$$aF + D_0 = 0, \tag{85}$$

where a is the flexibility matrix for the base structure, F is the column matrix of redundant forces to be determined, and D_0 is the column matrix of displacements under external loadings and temperature changes for $F = 0$.

The flexibility coefficients derived heretofore for each individual ring element are based upon an application of load measured in forces per lineal inch of ring circumference at the load line radius. This will not, in the general case, produce a symmetric flexibility matrix. In order to obtain a symmetric matrix, the already derived formulas will be amended to indicate displacements due to application of a total load of unit magnitude applied around the total circumference at the load line radius. With the indicated revisions, the

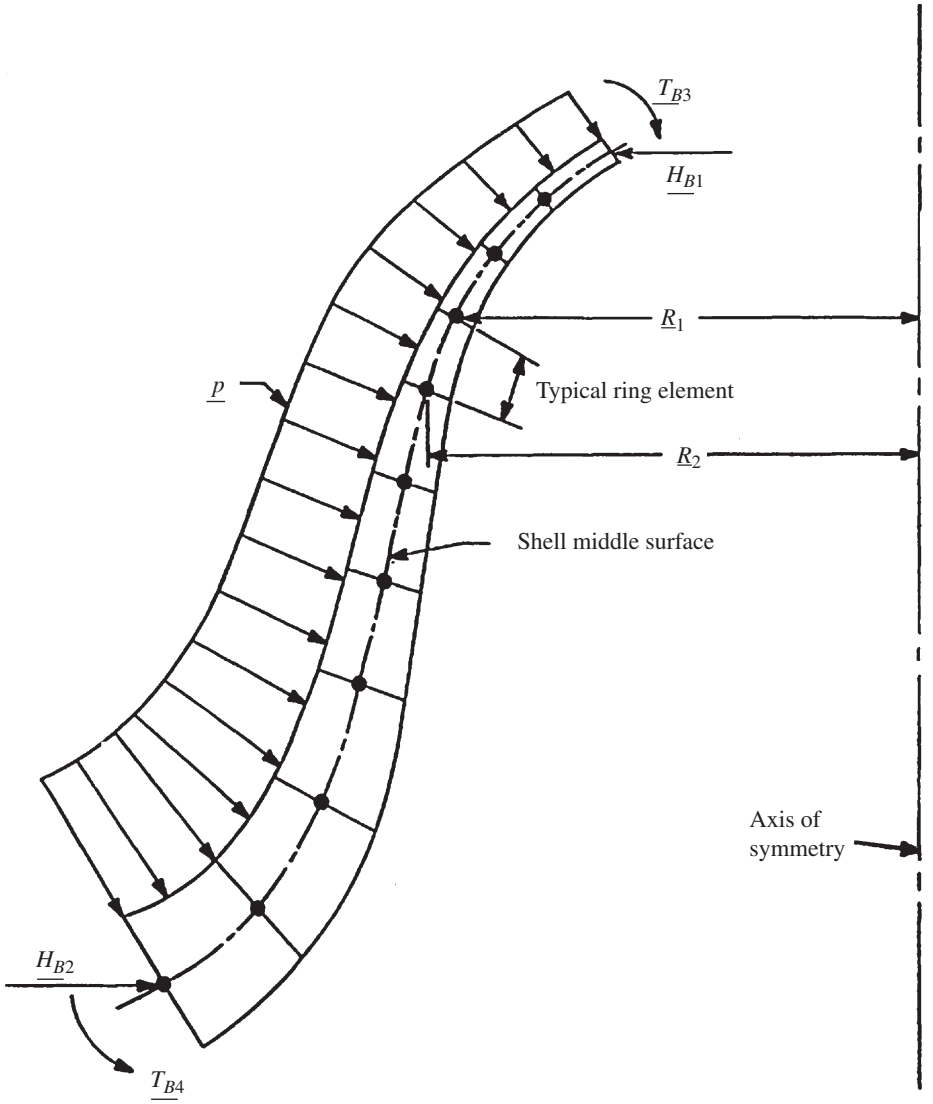

Fig. 12. Typical axisymmetric shell structure and loading. H_{B1} and H_{B2} are the radial boundary forces per unit circumferential length. T_{B3} and T_{B4} are the meridional moments per unit circumferential length at the shell boundaries.

flexibility coefficients for an individual ring element are finally obtained as follows:

$$\delta_{11} = \frac{R}{2\pi E}\left[\frac{c^2}{I_{z'}} + \frac{1}{A} + \frac{vc\ell^2 \sin\alpha\cos\alpha}{6RI_{z'}} + \frac{v\sin\alpha}{Rt} + \frac{\ell\sin^2\alpha}{3R^2t}\right], \tag{86a}$$

$$\delta_{21} = \delta_{12} = \frac{R}{2\pi E}\left[\frac{c\mathrm{d}}{I_{z'}} - \frac{1}{A} + \frac{\ell\sin^2\alpha}{3R^2t}\right], \tag{86b}$$

$$\delta_{31} = \delta_{13} = -\frac{R}{2\pi EI_{z'}}\left[c + \frac{v\ell^2 \sin\alpha\cos\alpha}{12R} + \frac{vc\ell\sin\alpha}{2R}\right], \tag{86c}$$

$$\delta_{41} = \delta_{14} = \frac{R}{2\pi EI_{z'}}\left[c + \frac{v\ell^2 \sin\alpha\cos\alpha}{12R} - \frac{vc\ell\sin\alpha}{2R}\right], \tag{86d}$$

$$\delta_{22} = \frac{R}{2\pi E}\left[\frac{d^2}{I_{z'}} + \frac{1}{A} - \frac{vd\ell^2 \sin\alpha\cos\alpha}{6RI_{z'}} + \frac{\ell \sin^2\alpha}{3R^2 t} - \frac{v\sin\alpha}{Rt}\right], \tag{86e}$$

$$\delta_{32} = \delta_{23} = \frac{R}{2\pi E I_{z'}}\left[-d + \frac{v\ell^2 \sin\alpha\cos\alpha}{12R} - \frac{vd\ell\sin\alpha}{2R}\right], \tag{86f}$$

$$\delta_{42} = \delta_{24} = \frac{R}{2\pi E I_{z'}}\left[d - \frac{v\ell^2 \sin\alpha\cos\alpha}{12R} - \frac{vd\ell\sin\alpha}{2R}\right], \tag{86g}$$

$$\delta_{33} = \frac{1}{2\pi E}\left[\frac{R}{I_{z'}} + \frac{v\ell\sin\alpha}{I_{z'}} + \frac{4\ell}{Rt^3}\right], \tag{86h}$$

$$\delta_{43} = \delta_{34} = -\frac{R}{2\pi E I_{z'}} + \frac{\ell}{\pi E R t^3}, \tag{86i}$$

$$\delta_{44} = \frac{R}{2\pi E I_{z'}} - \frac{vl\sin\alpha}{2\pi E I_{z'}} + \frac{2\ell}{\pi E R t^3}, \tag{86j}$$

where δ_{ij} represents the deflection in the ring coordinate i due to a unit value of force in coordinate j.

Our revised expressions for individual ring element axial deformations due to unit total circumferential values of the forces in the coordinate directions 1, 2, 3, and 4 are

$$\delta_{V1} = \delta_{1V} = \frac{R}{2\pi E}\left[\frac{c(R_2 - R_1)}{I_{z'}} + \frac{vl^2(R_2 - R_1)\sin\alpha\cos\alpha}{12RI_{z'}} - \frac{l\sin\alpha\cos\alpha}{2R^2 t} - \frac{v\cos\alpha}{Rt}\right], \tag{87a}$$

$$\delta_{V2} = \delta_{2V} = \frac{-R}{2\pi E}\left[-\frac{d(R_2 - R_1)}{I_{z'}} + \frac{v\ell^2(R_2 - R_1)\sin\alpha\cos\alpha}{12RI_{z'}} + \frac{\ell\sin\alpha\cos\alpha}{2R^2 t} - \frac{v\cos\alpha}{Rt}\right], \tag{87b}$$

$$\delta_{V3} = \delta_{Vv} = -\frac{R(R_2 - R_1)}{2\pi E I_{z'}}\left[1 + \frac{v\ell\sin\alpha}{2R}\right], \tag{87c}$$

$$\delta_{V4} = \delta_{4V} = \frac{R(R_2 - R_1)}{2\pi E I_{z'}}\left[1 - \frac{v\ell\sin\alpha}{2R}\right]. \tag{87d}$$

For the analysis of the structure, the base structure will be obtained by dividing the structure into a series of conical ring elements as indicated in Fig. 12. The separate ring elements will be numbered as indicated in Fig. 13, and the coordinate system for the redundant radial forces and moments will be selected as shown in Fig. 13.

The column matrix of unknown forces and moments can now be represented as

$$[F] = [P_1, P_2, \ldots, P_{N-1}, M_N, M_{N+1}, \ldots, M_{2N-3}, M_{2N-2}]^{\mathrm{T}}. \tag{88}$$

The column matrix of displacements for the base structure, with the redundants removed, can be represented as

$$[D_0] = [D_{10}, D_{20}, \ldots, D_{N-1,0}, D_{N,0}, D_{N+1,0}, \ldots, D_{2N-3,0}, D_{2N-2,0}]^{\mathrm{T}}. \tag{89}$$

The flexibility matrix for the structure is represented as

$$[a] = [a_{ij}], \quad \begin{array}{l} i = 1, \ldots, 2N-2, \\ j = 1, \ldots, 2N-2. \end{array} \tag{90}$$

The individual elements for the column matrix of displacements may be determined from the following formulas:

$$D_{n0} = \Delta_{20}^{(n)} + \Delta_{10}^{(n+1)}, \quad n = 1, 2, \ldots, N-1, \tag{91a}$$

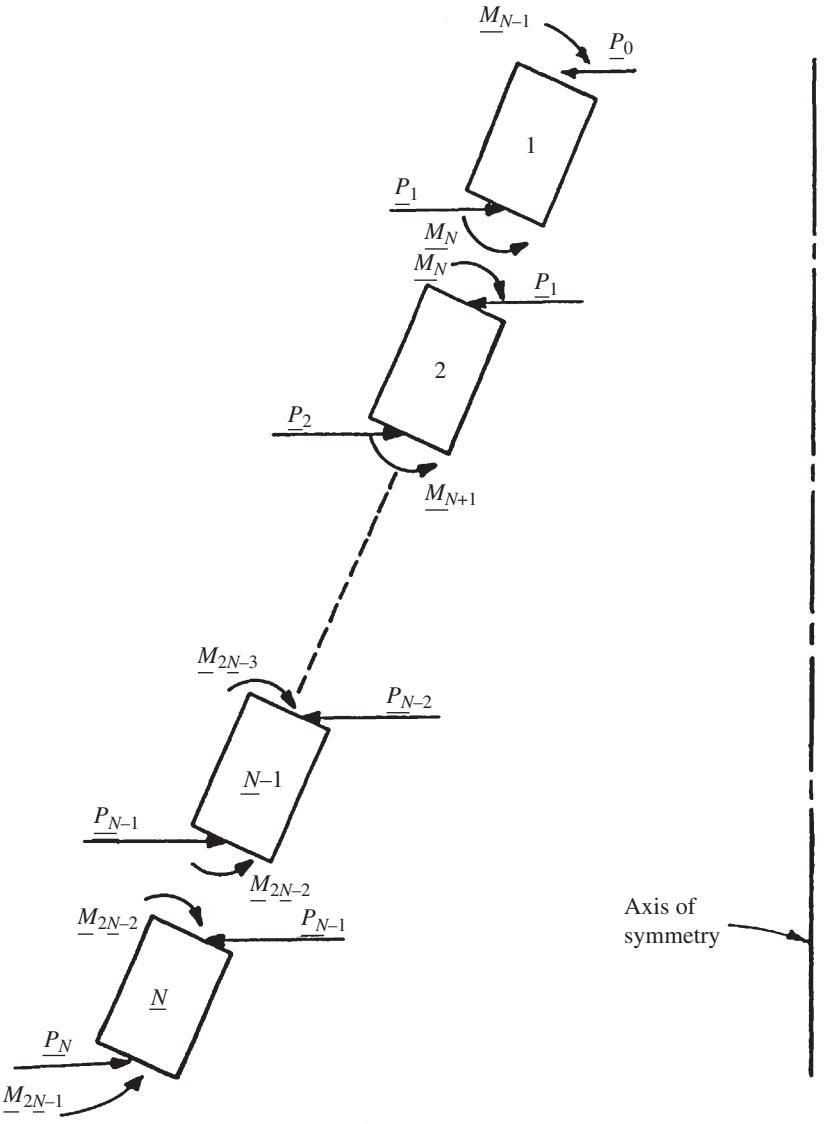

Fig. 13. Coordinate system for redundant radial forces and moments. $N =$ total number of ring elements. The boundary forces are $P_0 = 2\pi R_1 H_{B1}$ and $M_{N-1} = 2\pi R_1 T_{B3}$ at R_1 of ring element 1. They are $P_N = 2\pi R_2 H_{B2}$ and $M_{2N-1} = 2\pi R_2 T_{B4}$ at R_2 of ring element N. The forces $P_1 \leqslant P \leqslant P_{N-1}$ and $M_N \leqslant M \leqslant M_{2N-2}$ are the total circumferential redundant forces and moments.

$$D_{n0} = \Delta_{40}^{(n+1-N)} + \Delta_{30}^{(n+2-N)}, \quad n = N,\ N+1, \ldots 2N-2, \tag{91b}$$

where the quantity $\Delta_{20}^{(n)}$ typically represents the free ring deflection in the coordinate direction 2 for the ring associated with the ring number n.

The nonzero elements of the flexibility matrix may be determined from the following formulas:

$$a_{nn} = \delta_{22}^{(n)} + \delta_{11}^{n+1}, \quad n = 1, 2, \ldots, N-1, \tag{92a}$$

$$a_{nn} = \delta_{44}^{(n+1-N)} + \delta_{33}^{n+2-N}, \quad n = N,\ N+1, \ldots 2N-2, \tag{92b}$$

$$a_{n,n-1} = \delta_{21}^{(n)}, \quad n = 2, 3, \ldots, N-1, \tag{92c}$$

$$a_{n+1,n} = \delta_{43}^{(n+2-N)}, \quad n = N,\ N+1, \ldots, 2N-3, \tag{92d}$$

$$a_{N-1+n,n} = \delta_{42}^{(n)} + \delta_{31}^{n+1}, \quad n = 1, 2, \ldots, N-1, \tag{92e}$$

$$a_{N+n,n} = \delta_{41}^{(n+1)}, \quad n = 1, 2, 3, \ldots, N-2, \tag{92f}$$

$$a_{N-2+n,n} = \delta_{32}^{(n)}, \quad n = 2, 3, \ldots, N-1, \tag{92g}$$

$$a_{ij} = a_{ji}. \tag{92h}$$

The displacements at the nodal line coordinates for any ring element n may be obtained from

$$\begin{gathered} \Delta_j^{(n)} = P_{n-1}\delta_{j1}^{(n)} + P_n\delta_{j2}^{(n)} + M_{N+n-2}\delta_{j3}^{(n)} + M_{N+n-1}\delta_{j4}^{(n)} + \delta_{j0}^{(n)}, \\ n = 1, 2, 3, \ldots, N, \\ j = 1, 2, 3, 4, \end{gathered} \tag{93}$$

where $\delta_{j0}^{(n)}$ represents the displacements due to all effects except P and M.

The total axial deformation of the structure is obtained from

$$\Delta_{y'} = \sum_{n=1}^{N} \Delta_V^{(n)}. \tag{94}$$

The meridional stresses of interest for the boundary face of ring element 1 for the case of axial restraint at R_2 may be obtained from

$$\sigma_{y(AA)}^{(1)} = \frac{6T_{B3}}{t_1^{2(1)}} - \frac{L^{(1)}\cos\alpha^{(1)}}{t_1^{(1)}} - \frac{H_{B1}\sin\alpha^{(1)}}{t_1^{(1)}}, \tag{95a}$$

$$\sigma_{y(BB)}^{(1)} = -\frac{6T_{B3}}{t_1^{2(1)}} - \frac{L^{(1)}\cos\alpha^{(1)}}{t_1^{(1)}} - \frac{H_{B1}\sin\alpha^{(1)}}{t_1^{(1)}}. \tag{95b}$$

The meridional stresses of interest for interior ring elements, with axial restraint at R_2 of each element, may be obtained from

$$\sigma_{y(AA)}^{(n)} = +\frac{3M_{N+n-2}}{\pi R_1^{(n)} t_1^{2(n)}} - \frac{L^{(n)}\cos\alpha^{(n)}}{t_1^{(n)}} - \frac{P_{n-1}\sin\alpha^{(n)}}{2\pi R_1^{(n)} t_1^{(n)}}, \tag{96a}$$

$$\begin{gathered} \sigma_{y(BB)}^{(n)} = -\frac{3M_{N+n-2}}{\pi R_1^{(n)} t_1^{2(n)}} - \frac{L^{(n)}\cos\alpha^{(n)}}{t_1^{(n)}} - \frac{P_{n-1}\sin\alpha^{(n)}}{2\pi R_1^{(n)} t_1^{(n)}}, \\ n = 2, 3, \ldots, N. \end{gathered} \tag{96b}$$

The meridional stresses of interest for the boundary face of ring element N with axial load resisted at R'_2 may be found from

$$\sigma_{y(CC)}^{(N)} = \frac{6T_{B4}}{t_2^{2(N)}} - \frac{L^{(N)}R_1^{(N)}\cos\alpha^{(N)}}{R_2^{(N)}t_2^{(N)}} - \frac{p^{(N)}[R_2^{2(N)} - R_1^{2(N)}]\cos\alpha^{(N)}}{2R_2^{(N)}t_2^{(N)}} - \frac{H_{B2}\sin\alpha^{(N)}}{t_2^{(N)}}, \tag{97a}$$

$$\sigma_{y(DD)}^{(N)} = -\frac{6T_{B4}}{t_2^{2(N)}} - \frac{L^{(N)}R_1^{(N)}\cos\alpha^{(N)}}{R_2^{(N)}t_2^{(N)}} - \frac{p^{(N)}[R_2^{2(N)} - R_1^{2(N)}]\cos\alpha^{(N)}}{2R_2^{(N)}t_2^{(N)}} - \frac{H_{B2}\sin\alpha^{(N)}}{t_2^{(N)}}. \tag{97b}$$

It is emphasized here that the loadings L in Eqs. (95)–(97) include the contributions V_{p2} from preceding lower numbered ring elements as given by Eq. (55) and as shown in Fig. 8.

The circumferential strain, $\in_x$, may be determined for the points of interest on any ring from

$$\in_{x(AA)}^{(n)} = \frac{\Delta_1^{(n)} - \Delta_3^{(n)}[t_1^{(n)}/2]\sin\alpha^{(n)}}{R_1^{(n)} + (t_1^{(n)}/2)\cos\alpha^{(n)}}, \tag{98a}$$

$$\epsilon^{(n)}_{x(BB)} = \frac{\Delta^{(n)}_1 + \Delta^{(n)}_3[t^{(n)}_1/2]\sin\alpha^{(n)}}{R^{(n)}_1 - (t^{(n)}_1/2)\cos\alpha^{(n)}}, \tag{98b}$$

$$\epsilon^{(n)}_{x(CC)} = \frac{-\Delta^{(n)}_2 + \Delta^{(n)}_4[t^{(n)}_2/2]\sin\alpha^{(n)}}{R^{(n)}_2 + (t^{(n)}_2/2)\cos\alpha^{(n)}}, \tag{98c}$$

$$\epsilon^{(n)}_{x(DD)} = \frac{-\Delta^{(n)}_2 - \Delta^{(n)}_4[t^{(n)}_2/2]\sin\alpha^{(n)}}{R^{(n)}_2 - (t^{(n)}_2/2)\cos\alpha^{(n)}}, \quad n = 1, 2, 3 \ldots, N, \tag{98d}$$

where the subscripts 1, 2, 3, and 4 for Δ signify displacements in the directions 1, 2, 3, and 4 shown in Fig. 1.

The circumferential stresses, σ_x, may be determined for the points of interest on any ring element from

$$\begin{aligned} &\sigma^{(n)}_{x(j)} = E[\epsilon^{(n)}_{x(j)} - \beta Q^{(n)}] + \nu\sigma^{(n)}_{y(j)}, \\ &n = 1, 2, 3 \ldots, N, \\ &j = AA, BB, CC, DD. \end{aligned} \tag{99}$$

16. Comparison solutions for circular plate and cylindrical shell by the flexibility method and by the governing differential equations

The procedures that have been developed herein were programmed for the solution of actual cases by use of an electronic computer. In order to determine the accuracy of typical solutions by the flexibility method, the solution for a flat circular plate by the flexibility method will be compared with the solution obtained by use of the governing differential equations as a first case. This flat plate will be fixed at the outer edge and free at the inner edge. It will be loaded by a uniform load of 100.0 psi on the upper surface. The plate dimensions and loading are shown in Fig. 14.

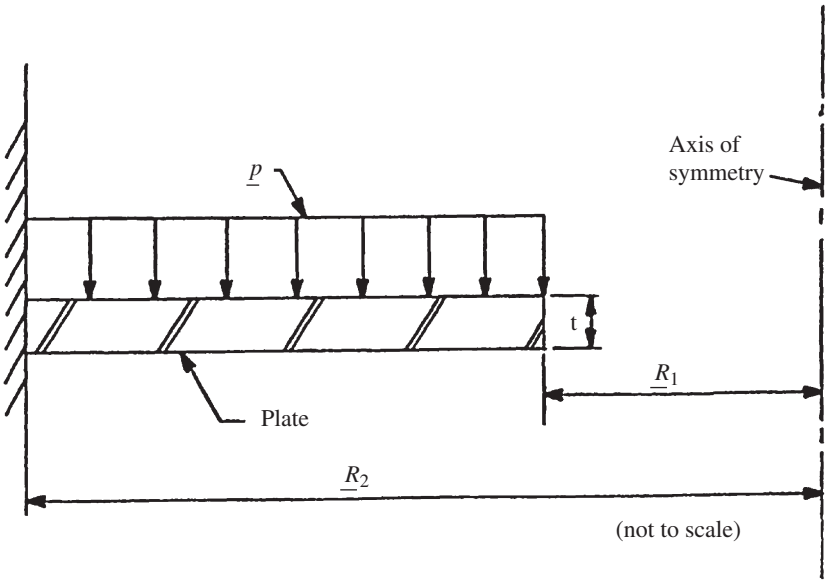

Fig. 14. Circular plate section and loading.
The loading $p = 100$ psi. Young's modulus $E = 30 \times 10^6$ psi. Poisson's ratio $\nu = 0.3$. The plate thickness $t = 0.25$ in. The inside radius $R_1 = 5.0$ in. The outside radius $R_2 = 8.0$ in. The inside boundary at R_1 is free of any restraint and the outside boundary at R_2 is fixed against any displacement.

Table 1
Circular plate solutions by the flexibility method

Radius (in.)	Δ_v (in.)	Δ_3 (rad)	$\sigma_{x(AA)}$ (psi)	$\sigma_{x(BB)}$ (psi)	$\sigma_{y(AA)}$ (psi)	$\sigma_{y(BB)}$ (psi)
5.00	0.01876	0.008771	−6578	6578	0	0
5.25	0.01658	0.008644	−6178	6178	−13	13
5.50	0.01444	0.008507	−5577	5577	569	−569
5.75	0.01233	0.008326	−4918	4918	1707	−1707
6.00	0.01028	0.008067	−4035	4035	3354	−3354
6.25	0.00831	0.007701	−2975	2975	5484	−5484
6.50	0.00644	0.007201	−1732	1732	8071	−8071
6.75	0.00472	0.006540	−305	305	11,093	−11,093
7.00	0.00319	0.005692	1310	−1310	14,533	−14,533
7.25	0.00189	0.004637	3113	−3113	18,374	−18,374
7.50	0.00088	0.003349	5105	−5105	22,602	−22,602
7.75	0.00023	0.001812	7284	−7284	27,205	−27,205
8.00	0	0	9651	−9651	32,173	−32,173

Table 2
Circular plate solutions by the differential equation method

Radius (in.)	Δ_v (in.)	Δ_3 (rad)	$\sigma_{x(AA)}$ (psi)	$\sigma_{x(\mathrm{BB})}$ (psi)	$\sigma_{y(\mathrm{AA})}$ (psi)	$\sigma_{y(\mathrm{BB})}$ (psi)
5.00	0.01867	0.008720	−6540	6540	0	0
5.25	0.01651	0.008597	−6144	6144	−12	12
5.50	0.01437	0.008464	−5600	5600	571	−571
5.75	0.01228	0.008286	−4893	4893	1704	−1704
6.00	0.01024	0.008031	−4014	4014	3351	−3351
6.25	0.00827	0.007669	−2957	2957	5481	−5481
6.50	0.00642	0.007173	−1718	1718	8068	−8068
6.75	0.00470	0.006516	−293	293	11,091	−11,091
7.00	0.00317	0.005674	1319	−1319	14,531	−14,531
7.25	0.00188	0.004624	3120	−3120	18,371	−18,371
7.50	0.00088	0.003342	5108	−5108	22,599	−22,599
7.75	0.00023	0.001808	7286	−7286	27,201	−27,201
8.00	0	0	9651	−9651	32,169	−32,169

The analysis by the flexibility method will be obtained by dividing the plate into 12 ring elements of one-fourth of an inch square cross section. Deflections, rotations, and stresses will thus be obtained at both boundaries and at intervals of one-fourth of an inch between the boundaries. The results obtained by the flexibility methods of this development are shown in Table 1.

The classical solution is found by solving the governing differential equations so as to satisfy the given boundary conditions. The solution by use of the governing differential equations is shown in Table 2.

It is seen by comparison of the solutions shown in Tables 1 and 2 that the results by the two methods are in remarkably good agreement at all locations and for all variables.

The second case to be considered will be a circular cylindrical shell free at both ends with the exception of an applied total radial load of 10,000 lb at the upper end of the cylinder. The cylinder dimensions and loading are shown in Fig. 15. The analysis by the flexibility method will be obtained by dividing the cylinder into 12 ring elements of 0.25 in. square cross section. Deflections, rotations, and stresses will be obtained at both boundaries and at 0.25 in. intervals between the boundaries. The results found by the flexibility method of this development are shown in Table 3.

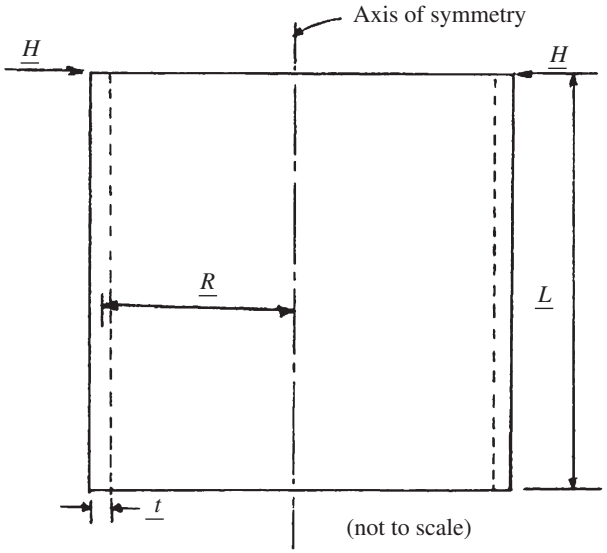

Fig. 15. Cylinder elevation and loading. The radius of the cylinder $R = 6.0$ in. Young's modulus $E = 30 \times 10^6$ psi. The length of the cylinder $L = 3.0$ in. Poisson's ratio $v = 0.3$. The wall thickness $t = 0.25$ in. The boundary at the base of the cylinder is free, and the boundary at the upper end of the cylinder is free with the exception of the total circumferential load $H = 10{,}000$ lbs.

Table 3
Cylindrical shell solutions by the flexibility method

z (in.)	Δ_1 (in.)	Δ_3 (rad)	$\sigma_{x(AA)}$ (psi)	$\sigma_{x(BB)}$ (psi)	$\sigma_{y(AA)}$ (psi)	$\sigma_{y(BB)}$ (psi)
0.00	−0.00272	0.002906	−13,358	−13,926	0	0
0.25	−0.00201	0.002745	−8422	−11,728	4810	−4810
0.50	−0.00137	0.002349	−4605	−9144	7087	−7087
0.75	−0.00085	0.001858	−1865	−6616	7623	−7623
1.00	−0.00045	0.001369	−58	−4395	7673	−7073
1.25	−0.00016	0.000935	1005	−2594	5942	−5942
1.50	0.00003	0.000583	1521	−1229	4593	−4593
1.75	0.00014	0.000321	1667	−262	3264	−3264
2.00	0.00020	0.000143	1594	376	2098	−2098
2.25	0.00022	0.000034	1418	760	1172	−1172
2.50	0.00022	−0.000022	1223	960	514	−514
2.75	0.00021	−0.000044	1064	1032	126	−126
3.00	0.00020	−0.000048	970	1011	0	0

The classical solution is obtained from the fourth-order differential equation with the constants of integration determined to satisfy the end boundary conditions. The results for the solution found from the fourth-order governing differential equation are shown in Table 4.

Comparison of the results given in Tables 3 and 4 shows again that the solutions are in generally very good agreement.

It is seen that the comparison solutions given in Tables 1 and 2 for the flat plate are in general in better agreement than the comparison solutions in Tables 3 and 4 for the cylindrical shell. This is of interest because Eqs. (18b), (19b), (23b), (27b), and (31b) for σ_y are "exact" as given for the cylindrical shell, whereas they involve the approximation that $(R_1 + s\sin\alpha) = R$ for the flat plate and all other ring elements for which $\alpha \neq 0$. We attribute these differences to truncation errors in the solution process with the carrying of only seven digits in the calculations.

Table 4
Cylindrical shell solutions by the differential equation method

z (in.)	Δ_1 (in.)	Δ_3 (rad)	$\sigma_{x(AA)}$ (psi)	$\sigma_{x(BB)}$ (psi)	$\sigma_{y(AA)}$ (psi)	$\sigma_{y(BB)}$ (psi)
0.00	−0.00268	0.002805	−13,411	−13,411	0	0
0.25	−0.00200	0.002644	−8525	−11,426	4835	−4835
0.50	−0.00138	0.002269	−4740	−9041	7168	−7168
0.75	−0.00087	0.001809	−2008	−6669	7768	−7768
1.00	−0.00047	0.001348	−187	−4550	7270	−7270
1.25	−0.00019	0.000939	905	−2797	6169	−6169
1.50	0	0.000605	1457	−1437	4822	−4822
1.75	0.00012	0.000354	1642	−440	3470	−3470
2.00	0.00018	0.000181	1606	248	2262	−2262
2.25	0.00022	0.000075	1465	696	1282	−1282
2.50	0.00023	0.000020	1306	963	571	−571
2.75	0.00023	0	1187	1101	143	−143
3.00	0.00023	−0.000003	1141	1141	0	0

17. Conclusions

It has been shown that the circumferential stresses (σ_x) in a ring element under axisymmetrically applied radial forces or edge moments can be determined "exactly" by simple flexuere formulas without any need to assume a stress or displacement field as is usually done in finite element analysis. It has also been shown that all significant bending and direct stresses (σ_y) in the meridional direction of the ring element due to radial forces and edge moments are found very closely by an assumption of a linear variation of stress between the boundary edges of the ring element.

It is seen by comparison of the solutions given in Tables 1 and 3 for solutions by the flexibility methods of this article and in Tables 2 and 4 for solutions obtained from the governing differential equations that the agreement is remarkably good at all node points and for all variables. Results not shown here or in Ref. [8] for actual shell structures of irregular meridional geometry and variable wall thicknesses have shown remarkably good agreement with test results.

We also mention a significant advantage of the procedures developed here over the more commonly used finite element methods of analysis in which the form of the displacement field is assumed. In this development, circumferential stresses in the ring element are computed directly by the "exact" formulae, Eqs. (8) and (10), thus leading to quite accurate influence coefficients that yield correspondingly accurate analytical results. The primary assumption used here in regard to meridional stresses is that, for the determination of influence coefficients, the meridional stresses vary linearly in the meridional direction of the element, a very good assumption for the expected dimensions of the ring thickness and distance between edges of the ring elements in the meridional direction of the shell.

It is concluded that the flexibility methods outlined herein may be used to obtain reliable and quite accurate values for the displacements and stresses in axisymmetric shell structures under axisymmetric loadings.

Acknowledgments

Acknowledgment is made to Mr. Grady E. Patrick, formerly employed by the US Army Missile Command, who programmed the equations developed in this article [9] for the analysis of axisymmetric shell structures.

Acknowledgment is extended also to Mr. Richard L. Rausch,[1] formerly employed by the U.S. Army Missile Command, who obtained the solutions for the plate example included herein by the differential equation method.

[1]Deceased.

References

[1] R.K. Penny, Symmetrical bending of the general shell of revolution by finite difference methods, *Journal of Mechanical Engineering Science* 3 (1961) 369–377.
[2] P.P. Radkowski, R.M. Davis, M.R. Bolduc, Numerical analysis of equations of thin shells of revolution, *ARS Journal* 32 (1962) 36–41.
[3] B. Budiansky, P.P. Radkowski, Numerical analysis of usymmetrical bending of shells of revolution, *AIAA Journal* 1 (1963) 1833–1842.
[4] A. Kalnins, Analysis of shells of revolution subjected to symmetrical and nonsymmetrical loads, *Transactions of the ASME 31E Journal of Applied Mechanics* 3 (1964) 467–476.
[5] A. Kalnins, Free vibration of rotationally symmetric shells, *Journal of the Acoustical Society of America* 36 (1964) 1355–1365.
[6] H. Kraus, A. Kalnins, Transient vibration of thin elastic shells, *Journal of the Acoustical Society of America* 38 (1965) 994–1002.
[7] J.H. Percy, T.H.H. Pian, S. Klein, D.R. Navaratna, Application of matrix displacement method to linear elastic analysis of shells of revolution, *AIAA Journal* 3 (1965) 2138–2145.
[8] T.A. Smith, Analysis of axisymmetric shell structures under axisymmetric loading by the finite element method, 1966 US Army Missile Command Technical Report RS-TR-66-8, Redstone Arsenal, Alabama, 1966.
[9] G.E. Patrick, Jr., Computer program for the analysis of axisymmetric shell structures under axisymmetric loading by the finite ring method, 1966 US Army Missile Command Technical Report RS-TR-66-9, Redstone Arsenal, Alabama, 1966.
[10] S. Klein, Vibrations of multi-layer shells of revolution under dynamic and impulsive loading, *Shock and Vibration Bulletin* 35 (1966) 486–494.
[11] T.A. Smith, Numerical solution for the dynamic response of rotationally symmetric shells of revolution under transient loadings, 1970 US Army Missile Command Technical Report RS-TR-70-5, Redstone Arsenal, Alabama, 1970.
[12] T.A. Smith, Numerical analysis of rotationally symmetric shells under transient loadings, *AIAA Journal* 9 (1971) 637–643.
[13] T.A. Smith, Implicit high-order finite difference analysis of rotationally symmetric shells, 1973 US Army Missile Command Technical Report RL-73-9, Redstone Arsenal, Alabama, 1973.
[14] H. Radwan, J. Genin, Nonlinear modal equations for thin elastic shells, *International Journal of Non-Linear Mechanics* 10 (1975) 15–29.
[15] T.A. Smith, Explicit high-order finite difference analysis of rotationally symmetric shells, 1977 US Army Missile Command Technical Report TL-77-1, Redstone Arsenal, Alabama, 1977.
[16] T.A. Smith, Explicit high-order finite difference analysis of rotationally symmetric shells, *AIAA Journal* 18 (1980) 309–317.
[17] Y.B. Chang, T.Y. Yang, W. Soedel, Linear dynamic analysis of revolutional shells using finite elements and modal expansion, *Journal of Sound and Vibration* 86 (1983) 523–538.
[18] T.A. Smith, Finite difference analysis of rotationally symmetric shells under discontinuous distributed loadings, 1983 US Army Missile Command Technical Report RL-83-5, Redstone Arsenal, Alabama, 1983.
[19] T.A. Smith, Finite difference analysis of rotationally symmetric shells under discontinuous distributed loadings, *AIAA Journal* 25 (1987) 1611–1621.
[20] T.A. Smith, Dynamic analysis of rotationally symmetric shells by the modal superposition method, 1991 US Army Missile Command Technical Report RD-ST-91-1, Redstone Arsenal, Alabama, 1991.
[21] T.A. Smith, Dynamic analysis of rotationally symmetric shells by the modal superposition method, *Journal of Sound and Vibration* 233 (2000) 515–543.
[22] G.R. Heppler, L. Wahl, Finite element analysis of free–free shells of revolution, *Journal of Sound and Vibration* 152 (2) (1992) 263–283.
[23] K.R. Sivadas, N. Ganesan, Dynamic analysis of circular cylindrical shells with material damping, *Journal of Sound and Vibration* 166 (1) (1993) 103–116.
[24] T.A. Smith, Improved explicit high-order finite difference analysis of rotationally symmetric shells, 1994 US Army Missile Command Technical Report RD-ST-94-12, Redstone Arsenal, Alabama, 1994.
[25] G. Sinha, M. Mukhopadhyay, Transient dynamic response of arbitrary stiffened shells by the finite element method, *Journal of Vibration and Acoustics* 117 (1995) 11–16.
[26] P.P. Goncalves, N.R.S.S. Ramos, Numerical method for vibration analysis of cylindrical shells, *ASCE Journal of Engineering Mechanics* 123 (1997) 544–550.
[27] J.L. Meek, Y. Wang, Nonlinear static and dynamic analysis of shell structures with finite rotation, *Computer Methods in Applied Mechanics and Engineering* 162 (1998) 301–315.
[28] T.A. Smith, Finite difference analysis of rotationally symmetric shells using variable node point spacings and incorporating matrix stability analysis, 1998 US Army Aviation and Missile Command Technical Report RD-PS-99-1, Redstone Arsenal, Alabama, 1998.
[29] T.A. Smith, Finite difference analysis of rotationally symmetric shells using variable node point spacings, *Journal of Sound and Vibration* 230 (2000) 1119–1145.
[30] W.R. Sellers, Jr., A mathematical library for your PC, 1988 US Army Missile Command Letter Report No. AMSMI-RD-SS-88-25, Redstone Arsenal, Alabama, 1988.
[31] T.A. Ozkul, A finite element formulation for dynamic analysis of shells of general shape by using the Wilson-0 method, *Thin-Walled Structures* 42 (2004) 497–513.
[32] S. Timoshenko, *Strength of Materials*, third ed., D. Van Nostrand Company, Inc., New York, 1955.
[33] J.A. Van den Broek, *Elastic Energy Theory*, Wiley, New York, 1942.